Cable-Driven Parallel Robot Modelling Considering Pulley Kinematics and Cable Elasticity

Thibaut Paty, Nicolas Binaud, Stéphane Caro, Stéphane Segonds

Cable-Driven Parallel Robot Modelling Considering Pulley Kinematics and Cable Elasticity

Thibaut Paty[a,*], Nicolas Binaud[a], Stéphane Caro[b], Stéphane Segonds[a]

[a] *Institut Clément Ader (ICA), Université de Toulouse, CNRS/INSA/ISAE/Mines Albi/UPS, Toulouse, France*
[b] *CNRS, LS2N, UMR CNRS 6004, Nantes, France*

Abstract

Cable Driven Parallel Robots (CDPRs) are parallel robots, in which the limbs are replaced by cables that are guided by pulleys. In many papers, the pulleys are considered as fixed points of passage and the cable elasticity is neglected. Those approximations simplify the robot modelling, but lead to some Moving-Platform (MP) pose errors. This paper deals with the modelling of suspended CDPRs considering the geometry and kinematics of the pulleys as well as the cable elasticity. Furthermore, a novel pulley architecture with an universal joint is designed. It is introduced to increase the accuracy of CDPRs and limit the bending moment in the pulleys. Then a sensitivity analysis conducted on these newly established models allows to precisely quantify the effect of design parameters on the MP pose and to exhibit the set of the most influentials elasto-geometric parameters. Both standard and extended direct elasto-geometric static models of the CDPRs are numerically solved to determine the MP pose for given cable lengths and external wrench. Then, an index is defined based on the MP pose difference, the latter being traced through the robot Cartesian workspace. This index is used to analyze and compare the pulleys effects on the MP pose errors. It turns out that the interaction between pulleys geometrical parameters are significant and should be considered in the elasto-geometric static models. Finally, it is shown that a CDPR equipped with the novel pulley architecture is more sensitive to cable elasticity, but this new architecture helps reducing the overall MP error.

Keywords: Cable-driven parallel robot, Pulleys, Cables elasticity, Accuracy, Sensitivity analysis.

1. Corresponding author: Thibaut Paty; Email: thibaut.paty@univ-tlse3.fr

1. Introduction

Parallel robots are closed kinematic chain mechanisms whose Moving-Platform (MP), is connected to the base with several limbs. Parallel robots have higher stiffness and dynamic performance than their serial counterparts thanks to the closed kinematic chains and to the actuators usually mounted to the base [1]. These mechanisms are mainly used for high-speed pick-and-place applications or to move a high payload in a small workspace [2, 3]. On the contrary, the Cable-Driven Parallel Robots (CDPRs) have a large workspace, have a simple design and can have a high payload capacity as well as good dynamic performance thanks to their actuators mounted to the ground and their long cables [4, 5]. There have been many studies on CDPRs the last twenty years due to their multiple and varied applications [6, 7]. Here are some CDPR application cases : surface finishing [8], additive manufacturing of large parts [9], camera displacement for filming sports events [10] and even one part of a giant radio telescope [11]. CDPRs are usually composed of a fixed frame, a set of actuators and winches mounted to the ground, a MP and cables that connect the latter to the winches via pulleys. [12]. They can be planar or spatial [13, 14]. Moreover, it is possible distinguish two CDPRs families. Firstly, suspended CDPRs where the cables come from above the MP and their number can be equal (non-redundant) or superior (redundant) than the number of degrees of freedom (Dof) of the CDPR [15]. In this case, gravity plays an important role while pulling the MP downward and as a consequence keeping the cables in tension. The second family gathers the fully-constrained CDPRs, which can apply forces and moments onto the MP along and about all axes [16].

It is interesting to note that the advantages attributed by the cables also introduce some drawbacks. Main CDPRs defects their low accuracy [17, 18] and their vibrations [19]. For CDPRs, the Inverse Geometric static Model (IGM) is relatively simple to obtain, but the Direct Geometric static Model (DGM) is much more difficult to solve [20]. This can be an issue for the control of the MP pose in the Cartestian space [21]. To help resolve the DGM, the idler pulleys of cable are simplified by modelling them by fixed passage points [16]. Under this assumption, the so-called “standard” geometric static models have been developed. In reality, during the modification of cable lengths the winding lengths of cables on the pulleys vary and the exit points of the cables are not fixed [22]. Therefore, the solution obtained with geometric static models differs from those produced by models taking into account pulleys called "extended" models [23]. In addition, in standard geometric models, the cables are considered to be non-deformable and straight [24]. For the design and control of CDPRs the standard geometrical static models are mostly used [25, 26]. The following paper focuses on the influence of pulleys geometric parameters and cable elasticity on the MP pose. To do this, the standard geometrico static model and the extended elasto-geometrico static models of the robot are computed and an index is defined based on the difference between the computed MP poses. This index is used to analyse and compare the effects of two types of pulley architectures on the MP pose estimation. The design of a novel pulley architecture aiming at improving CDPR accuracy is also presented. Baklouti *et al.* [27] analyzed the sensitivity of CDPRs elasto-geometrico static models to geometrical and mechanical uncertainties. The authors show that the cables elasticity and more specifically the hysteresis effect of Young modulus between the strain and the sagging of the cables cannot be neglected. Therefore, in this paper, the sensitivity of the proposed extended models is analyzed with respect to variations in the cable Young modulus of elasticity.

Among the different possible configurations of spatial CDPRs, this paper focuses on suspended CDPRs having a MP as a point mass, for a matter of simplicity. The paper is organised as follows.

Section 2 deals with the CDPR modelling. Section 3 investigate the MP pose errors. The section 4 analyse the pulleys parameters influence. Section 5 presents the effects of cable elasticity variability.

2. CDPR modelling

The first step is to define the models used throughout the study. There are two types of models, the standard being commonly used in the literature and the extended, which takes into account the pulleys as well as the cable elasticity. First, the standard geometric model is remind and then, the extended models are described.

2.1. Standard geometric model

In the standard geometric definition of CDPR, the pulleys are simplified by modelling them as fixed passage points noted A_i, with $i = 1, \ldots, m$, where m being the number of cables of the CDPR. The Standard Inverse Geometric Models (IGM_S) is used to determine the length l_S^i between the cable exit points A_i and anchor points B_i for a given MP pose, as shown in Fig. 1. In addition, the cable length connecting the points A_i with the exit point of the winch, noted C_i, is taken into account. It should be noted that in the context of this study, C_i is assumed to be fixed and the vectors $\mathbf{a}_i$ collinear with $\mathbf{z}_b$ axis. The use of winches with an exit point of the cables imposed by a guide allows to respect this assumption [28]. This length is called the dead length l_d^i. In the IGM_S the cables are considered as non-elastic, massless and straight. The cable length vectror l_s^i is expressed by the i^{th} loop-closure equations, namely :

$$\mathbf{l}_S^i = \mathbf{p} + \mathbf{R}\mathbf{b}_i - \mathbf{a}_i - \mathbf{c}_i \quad \text{for } i = 1, \ldots, m \tag{1}$$

Where the norm of $\mathbf{l}_S^i$ is the standard useful length l_S^i of i^{th} cable. $\mathbf{p}$ is the position vector connecting the point O, center of the base frame $\mathcal{F}_b$, to the point P which is the geometric center of the MP. $\mathbf{R}$ from the base frame $\mathcal{F}_b$ to the MP frame $\mathcal{F}_p$. $\mathbf{b}_i$ is the vector pointing from the MP geometric center P to the cable anchor point B_i. $\mathbf{a}_i$ and $\mathbf{c}_i$ are the vectors pointing from C_i to A_i and from O to C_i, respectively.

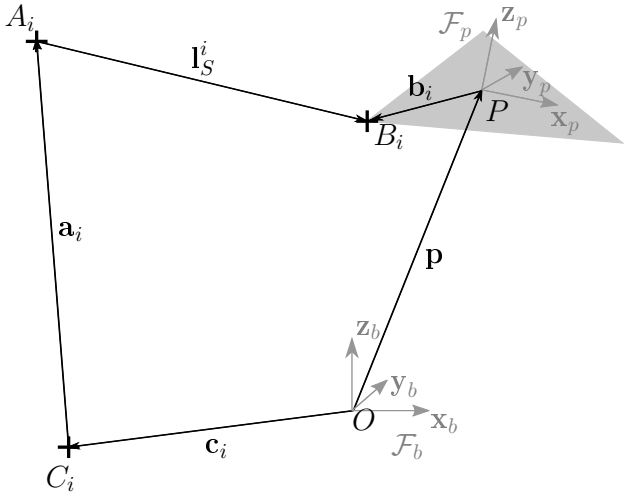

Figure 1 – Parameterization of a CDPR

The dead length l_d^i is 2-norm of vector $\mathbf{l}_d^i$ pointing from point C_i to point A_i. In the standard modelling this vector is constant whatever the MP pose, that is, $\mathbf{l}_d^i = \mathbf{a}_i$. Since the study is complemented by this dead length, the standard total length of cable i, noted $L_{T_S}^i$, to be considered expressed as :

$$L_{T_S}^i = \|\mathbf{l}_S^i\|_2 + \|\mathbf{l}_d^i\|_2 \quad , i = 1, \ldots, m \tag{2}$$

2.2. Extended elasto-geometrico model

In this study, the extended elasto-geometrico model consists in considering the pulley geometry and cable elasticity in the CDPR modelling. Two types of pulley geometry are presented, in order to analyze their impact on accuracy. First, the pulleys with only one revolute joint at the baseplate are presented, then the novel pulleys equipped with two revolute joints.

2.2.1. IGM_E with single revolute joint pulley

The majority of the CDPR using idler pulleys are equipped with single revolute joint models limiting the twisting of the cable like the CDPR prototype CAROCA [27]. This type of pulley allows a rotation around the $\mathbf{z}_b$ axis and the entry point of the cable is stationary, the aim being to align the cable with the rotation axis of the baseplate.

The installation of these pulleys can generate some difficulties, mainly during the passage of the cable in the sheave if it is equipped with a fixing ring, for example. In the aim to have removable CDPR for a fast re-assembly [29], it is necessary to use conventional pulleys, that eases their implementation. In these studies, it is analysed whether such pulleys can be used in the CDPR design. This is why the parameterization of this single revolute joint pulley has a pulley radius r_{p_i} and a lever arm h_i, like the pulley (articulated pulleys with support plates, PA6/7) of the manufacturer Huchez^{TM} (see Fig. 2a). It should be noted that the entry point of cable is no confused with the rotation axis of the pulley baseplate. The parametrization of this type of pulley is shown in Fig. 2b.

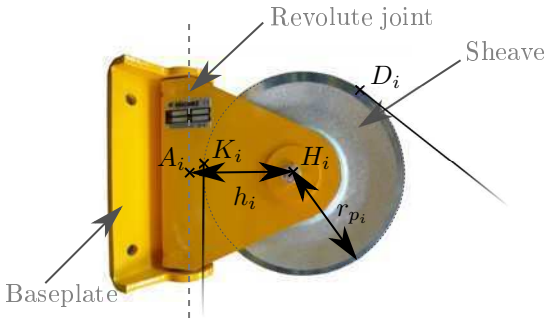

(a) Example of a pulley with a single revolute joint (PA6/7 Huchez^{TM})

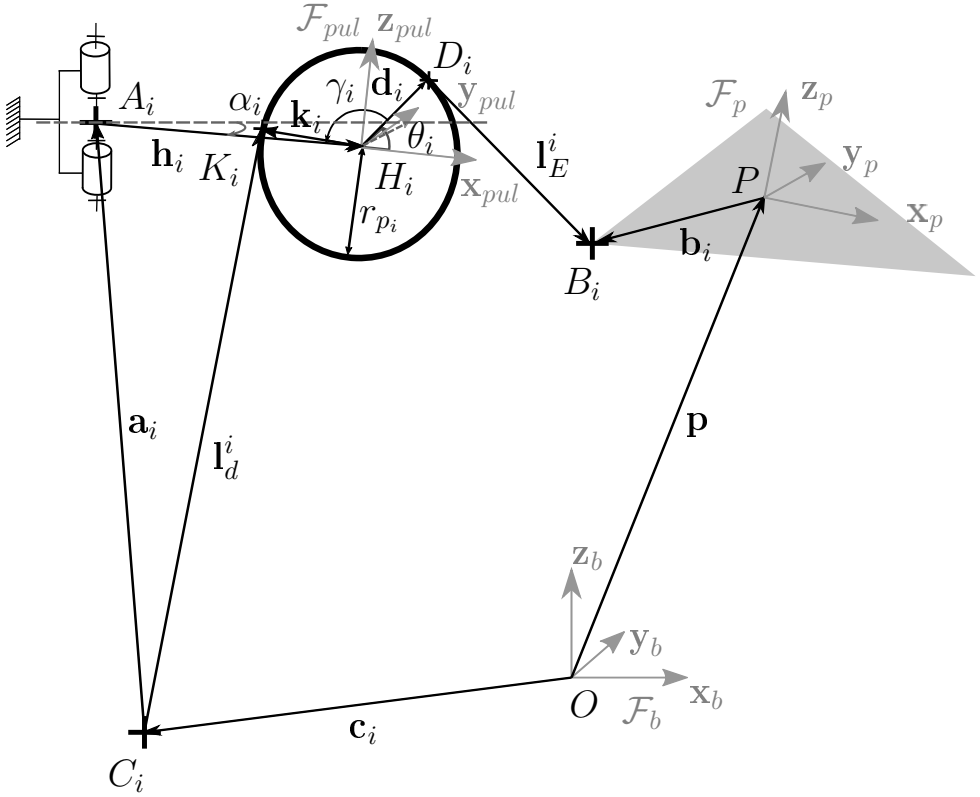

(b) Extended model parametrization with single revolute joint pulley of a m cables CDPR

FIGURE 2 – Parametrization of single revolute joint pulley

An orientation angle α_i of the pulley is therefore to be taken into account for the definition of the CDPR geometry. Pulley geometry is defined by its radius r_{p_i}, the length h_i between the fixed point A_i of the revolute joint and the pulley center H_i. This length is called lever arm of the

pulley and is defined by the 2-norm of the vector $\mathbf{h}_i$. The angle α_i is a function of the MP pose and must respect the static equilibrium of CDPR as well as the position of the exit point of the cable from the point D_i. The extended useful length l_E^i is descripted by the 2-norm of the vector l_E^i connecting the point D_i to point B_i. Vectors $\mathbf{l}_E^i$ and $\mathbf{d}_i$ are perpendicular to each other, where $\mathbf{d}_i$ is the vector pointing from the pulley center H_i to tangent point D_i. The vector $\mathbf{l}_E^i$ describing the IGM_E is therefore written as :

$$\mathbf{l}_E^i = \mathbf{p} + \mathbf{R}\mathbf{b}_i - \mathbf{a}_i - \mathbf{c}_i - \mathbf{h}_i - \mathbf{d}_i \quad \text{for } i = 1, \ldots, m \tag{3}$$

with

$$\mathbf{h}_i + \mathbf{d}_i = [h_i + r_{p_i}\cos(\theta_i)][\cos(\alpha_i)\mathbf{x}_b - \sin(\alpha_i)\mathbf{y}_b] + r_{p_i}\sin(\theta_i)\mathbf{z}_b \tag{4}$$

θ_i is the angle beetween $\mathbf{d}_i$ and the $\mathbf{x}_{pul}$ axis of the $\mathcal{F}_{pul}$ coordinate systems attached to the pulley. In addition to knowing $\mathbf{l}_E^i$, in order to determine the extended total length $L_{T_E}^i$ of the deployed cable i, it is now necessary to know $\mathbf{l}_d^i$ as well as the cable winding length around the pulley. Let us note that here $\mathbf{l}_d^i$ is no longer collinear with $\mathbf{a}_i$ and is no longer constant because it depends on the MP pose. In the majority of the CDPR prototypes the exit point C_i of the winches is fixed with winch models with guiding of the cable [28] and it is collinear with the axis of the pulley revolute joint. This has the effect of avoiding too important variation in the curvature of the cable because it always belong to the plane (H_i, $\mathbf{x}_{pul}$, $\mathbf{z}_{pul}$) and its entry into the pulley is tangent to the outside diameter. It has thus always an alignment of the pulley with the point B_i of the MP. In this configuration, to determine $\mathbf{l}_d^i$, it is possible to verify that the position of the entry point of cable into the pulley K_i is constant in the $\mathcal{F}_{pul}$ coordinates systems of the pulley, K_i is defined by the vector $\mathbf{k}_i$. Indeed, as $\mathbf{a}_i$ and $\mathbf{z}_b$ are considered collinear, the angle between $\mathbf{a}_i$ and $\mathbf{l}_d^i$ is always the same. This shows that the norm $\|\mathbf{l}_d^i\|_2$ is constant and thus is independent from the MP pose. On the other hand, for the part of the cable wound on the pulley, this length is function of the MP pose because it is described by the angle γ_i separating $\mathbf{k}_i$ and $\mathbf{d}_i$ as well as by the pulley radius r_{p_i}. The extended total length deployed is then :

$$L_{T_E}^i = \|\mathbf{l}_E^i\|_2 + \|\mathbf{l}_d^i\|_2 + \gamma_i r_{p_i} \quad \text{for } i = 1, \ldots, m \tag{5}$$

with $\gamma_i r_{p_i}$ the length of the cable wounded on the pulley i.

2.2.2. IGM_E with double revolute joint pulley

In the aim of mass-reduction and facilitating transportation of CDPR [29], that is, mountable easily and quickly, the use of the double revolute joint pulley, as shown in Fig. 3, can be an economically interesting solution, which have never been used in the design of CDPRs.

FIGURE 3 – Pulley for climbing activity (Pulley Xinda Rock Climbing)

Indeed, this type of pulley has many advantages like its cost, or its easier assembly/disassembly due to the type of fixation that does not necessarily need to be bolted. In addition, it also cancels the bending in the lever arm of length h_i. There is therefore a problem with the joint of the baseplate, because of the rotation of the pulley around the $\mathbf{x}_{pul}$ axis, and this rotation may cause strong torsion in the cable. Indeed, it is important to keep the cable plane formed by the vectors $\mathbf{l}_d^i$ and $\mathbf{l}_E^i$ always vertical to limit its torsion so one solution is to fix the rotation around $\mathbf{x}_{pul}$ and thus obtain a universal joint (U-joint) type at the baseplate (see Fig. 4a). This pulley can be displaced using two rotations axes, whose parameters are α_i and β_i (see Fig. 4b).

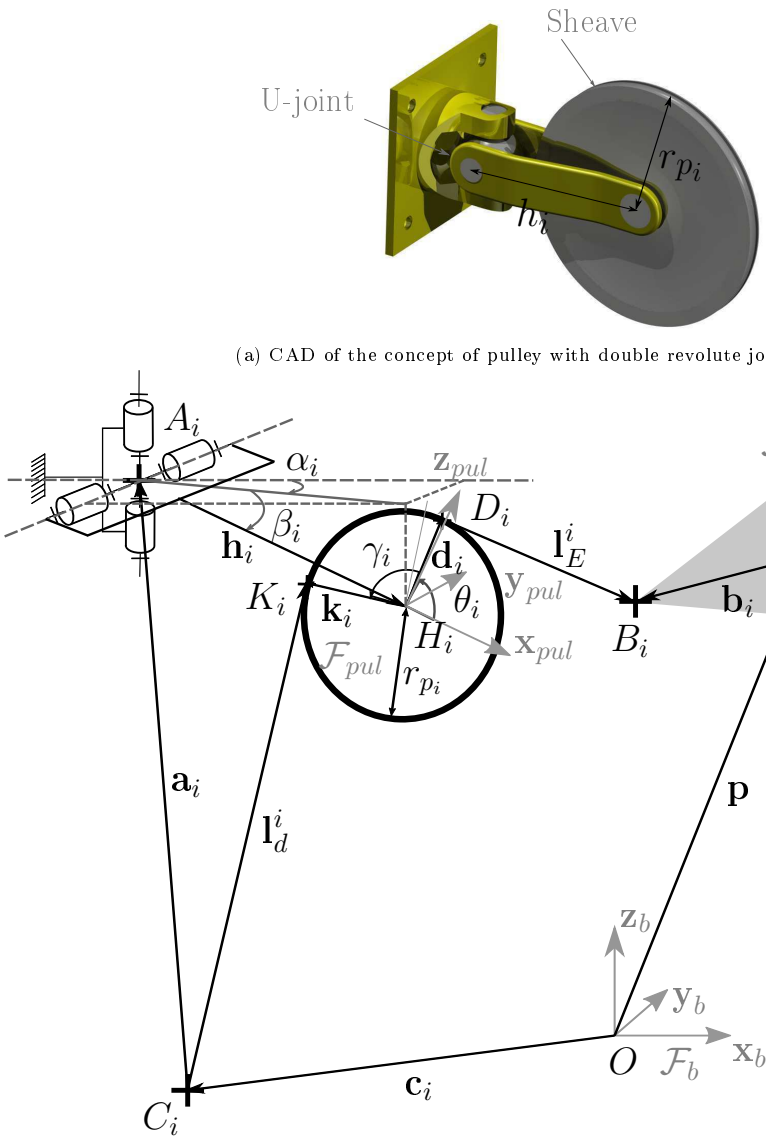

(a) CAD of the concept of pulley with double revolute joint

(b) Extended model parametrization of a m cables CDPR with double revolute joint pulley

FIGURE 4 – Presentation and parametrization of double revolute joint pulley

Figure 4b shows the setting of the double revolute joint pulley. The calculation of the orientation angle of the two revolute joints, α_i and β_i, are now necessary to determine the position of the pulley center H_i. β_i is the angle formed between the horizontal plane $(O, \mathbf{x}_b, \mathbf{y}_b)$ and $\mathbf{h}_i$, it is thus a function of the MP pose and must respect the static equilibrium of CDPR. Assuming that friction forces and pulley weight can be neglected in from of tensions in cables, and due to static equilibrium of forces, H_i must be on the bisector of the angle between $\mathbf{a}_i$ and $\mathbf{l}_S^i$, noted ϕ_i, as shown in Fig. 5.

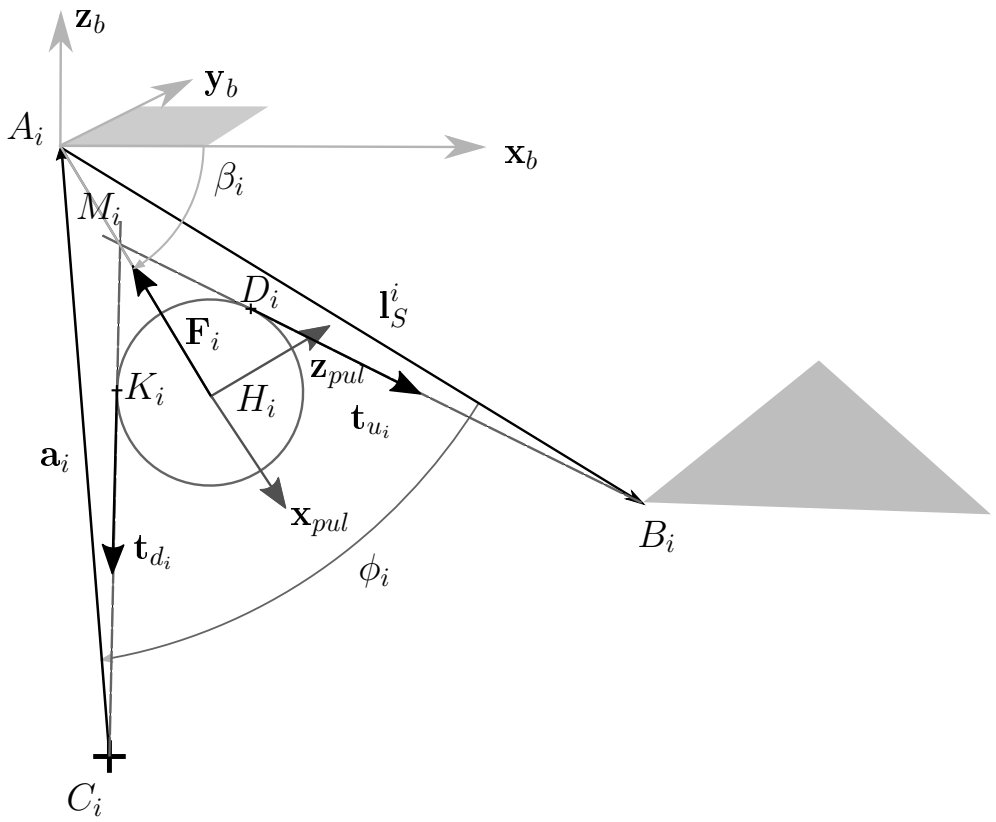

FIGURE 5 – Free-body diagram of a double revolute joint pulley

$\mathbf{t}_{d_i}$ and $\mathbf{t}_{u_i}$ represent the tensions in the cables at both ends of the pulley sheave and $\mathbf{F}_i$ the holding force in the lever arm of the pulley. Based on this principle, the IGM$_E$ with double revolute joint pulley calculating the useful length of cable is determined with the same vector chain as in Eq. (3). However, in this configuration, the sum of vectors $\mathbf{h}_i + \mathbf{d}_i$ is written :

$$\mathbf{h}_i + \mathbf{d}_i = [(r_{p_i}\cos(\theta_i) + h_i)\cos(\beta_i) + r_{p_i}\sin(\theta_i)\sin(\beta_i)](\cos(\alpha_i)\mathbf{x}_b - \sin(\alpha_i)\mathbf{y}_b) - [(r_{p_i}\cos\theta_i + h_i)\sin\beta_i - r_{p_i}\sin\theta_i\cos\beta_i]\mathbf{z}_b \quad (6)$$

Like in the single revolute joint model, the total length $L^i_{T_E}$ is calculated with Eq. (5). The difference is that the dead length l^i_d is not constant, the entry point of the cable into the pulley K_i being a function of the MP pose, $\|\mathbf{l}^i_d\|_2$ for $i = 1, \ldots, m$ is thus expressed :

$$\|\mathbf{l}^i_d\|_2 = \sqrt{\left[h_i sin\left(\frac{\phi_i}{2}\right)\right]^2 + \left[\mathbf{a}_i\mathbf{x}_b - h_i cos\left(\frac{\phi_i}{2}\right)\right]^2 - r_{p_i}^2} \quad (7)$$

2.2.3. Extended Direct Elasto-Geometrico Model ($DEGM_E$)

$DEGM_E$ allows to obtain the MP pose taking into account the pulleys and the cables elasticity for a cable length obtained with the IGM_S. To obtain the pose error between the standard and extended model it is necessary to solve the $DEGM_E$. The determination of the standard direct geometric model being already complex, the addition the geometric parameters of pulleys and the cable elasticity makes analytical resolution very difficult. A numerical resolution by successive iterations of the elasto-geometrico parameters is then used. This section describes a methodology for solving the $DEGM_E$ of CDPRs. To solve the $DEGM_E$ it is necessary to explain first the Extended Direct Geometric Model (DGM_E) and add elasticity afterwards. The cable lengths used in the DGM_E are the $L^i_{T_S}$ where $i = 1, \ldots, m$. For a matter of simplicity, Free-body diagram of a MP is supposed to be a point mass, denoted as P. Due to pulleys the incoming and outgoing cable must always be tangent to the outer diameter of the pulley and the pulley orientation with single or double revolute joint must fit respect the static equilibrium of CDPR. To solve the $DEGM_E$, the intersections between the spheres of center H_i and radius R_i are computed. Here are the spheres equations :

$$R_i = \sqrt{(L^i_{T_S} - \|\mathbf{l}^i_d\|_2 - \gamma_i r_{p_i})^2 + {r_{p_i}}^2} \quad \text{for } i = 1, \ldots, m \tag{8}$$

This is translated analytically by the m equations following system :

$$\begin{cases} (p_x - h_{x_1})^2 + (p_y - h_{y_1})^2 + (p_z - h_{z_1})^2 = (L^1_{T_S} - \|\mathbf{l}^1_d\|_2 - \gamma_1 r_{p1})^2 + {r_{p_1}}^2 \\ \vdots \\ (p_x - h_{x_m})^2 + (p_y - h_{y_m})^2 + (p_z - h_{z_m})^2 = (L^m_{T_S} - \|\mathbf{l}^m_d\|_2 - \gamma_m r_{p_m})^2 + {r_{p_m}}^2 \end{cases} \tag{9}$$

With $\mathbf{h}_i = (h_{x_i}\ h_{y_i}\ h_{z_i})^T$ and $\mathbf{p} = (p_x\ p_y\ p_z)^T$ where p_x, p_y, and p_z are solutions of the equation system Eq. (9), and represent the coordinates of the points P_{DGM_k} which are the accessible positions of the MP. In the case of a three cables CDPR, it should be noted that there are two solutions, $k = 1, 2$. The cables only work in tension, so only one of the solutions is physically accessible, this is the "low" solution that is retained, which denoted as P_{DGM_E}. However, when observing the system of Eq. (9) it possible to see that p_x, p_y and p_z are unknowns but the set of $\mathbf{h}_i = (h_{x_i} h_{y_i} h_{z_i})^T$ representing the pulleys center is also. Unlike their rigid segment counterpart, it is necessary to complete the system of Eq. (9) with the statics equations to come up with a determined system of equations. The new equation system allows to determine the DGM_E, and numerical method of successive iterations of the geometrical approah is used. That is to say, during the first calculation of P_{DGM_E}, noted $P^0_{DGM_E}$, the initial conditions of the pulley position, with single or double revolute joint according to the studied case, are drawn of the IGM_E for a given theoretical position P. The recalculation of the pulleys parameters is carried out in order to satisfy the static equilibrium constraints. At the end of this first recurrence $P^1_{DGM_E}$ is determined. $\mathbf{p}^j_{DGM_E}$ is the postion vector of the point $P^j_{DGM_E}$ in the base frame $\mathcal{F}_b$ at the iteration j. The stop condition is then checked, if $\|\mathbf{p}^j_{DGM_E} - \mathbf{p}^{j-1}_{DGM_E}\|_2 < \varepsilon_P$, if this is not the case additional iteration is carried out. When the stop condition is respected, at the iteration j=q, it is considered that $P^q_{DGM_E}$ is solution of the DGM_E.

Now, it is possible to enrich the extended models with the cable elasticity. The cable physics is one of the main topics in CDPR research, because it is very complex. Indeed, the cable can have several behaviour modes, i.e. sag or not by its self-mass and with the possibility to take into account its elasticity. For long cables, their mass cannot be neglected. Nguyen and al. [17] analysed

the influence of the mass and the elasticity in a complete model of sagging cable. In this study, the lengths of cables do not exceed a few meters and their diameters is sufficiently small to be able to neglect their mass and thus the sagging. However, having a small cross-section of cable amplifies the phenomenon of elongation thereof when the tensions of cables increase because of the displacement of a heavy load for example. The cable elasticity is therefore a significant parameter in the analysis of the CDPR accuracy. In the DEGM$_E$ presented in this paper, the cables are modelled by straight line segments and non-null elasticity. It is possible to model the elasticity via the Hooke's law

$$\sigma_i = E\epsilon_i \tag{10}$$

Where σ_i is the constraint of the i cable, $\epsilon_i = \frac{\Delta L_T^i}{L_T^i}$ its deformation and E its Young's modulus. It is shown in [27] that E has a non-linear evolution with respect to the loading of the cable and suffers from a hysteresis phenomenon between the loading and the unloading. As a first step, E is supposed to be constant, its variation will be modelled in the section 5. To be able to know the elongation ΔL_T^i, it is necessary to determine the tension in the cable. It is thus necessary to solve the static equilibrium equation of the MP [30] :

$$\mathbf{W}\mathbf{t} + \mathbf{w}_{ext} = \mathbf{0} \tag{11}$$

Where $\mathbf{t}$ is the cable tension vector and $\mathbf{w}_{ext}$ is the external wrench applied to the MP and $\mathbf{W}$ is the wrench matrix. In this article, the MP being modelled by a mass point the $\mathbf{b}_i$ are null, $\mathbf{W}$ is thus written simply according to the useful lengths of the extended parametrization $\mathbf{l}_E^i$. The simplified $\mathbf{W}$ matrix is denoted $\mathbf{M}$:

$$\mathbf{M} = -\begin{pmatrix} \frac{\mathbf{l}_E^1}{\|\mathbf{l}_E^1\|_2} & \dots & \frac{\mathbf{l}_E^m}{\|\mathbf{l}_E^m\|_2} \end{pmatrix} \tag{12}$$

The studied CDPR are suspended and reduced to a CDPR with n Dofs equal to m cables, it is therefore always possible to have a $\mathbf{M}$ square matrix to avoid matrix inversion problems. Finally, the elongation of the cable is written :

$$\Delta L_T^i = \frac{t_i L_T^i}{ES_i} \quad \text{for } i = 1, \dots, m \tag{13}$$

Where S_i is the cross section of the i^{th} cable. From the initial position $P^0_{DEGM_E}$ which corresponds to the position P_{DGM_E} determined with the DGM$_E$ and knowing the elongation of the each cable, it is then possible thanks to the DEGM$_E$ to recalculate the new MP position, that is, $P^1_{DEGM_E}$. However, at this new position the tensions of the vector $\mathbf{t}$ are modified and thus also the elongation of the cables. A numerical resolution by iterations is used again. The stop criterion at the iteration j is $\|\mathbf{p}^j_{DEGM_E} - \mathbf{p}^{j-1}_{DEGM_E}\|_2 < \varepsilon_P$. The diagram Fig. 6 illustrates the obtention of the final P_{DEGM_E} with the cable length determined with the IGM$_S$.

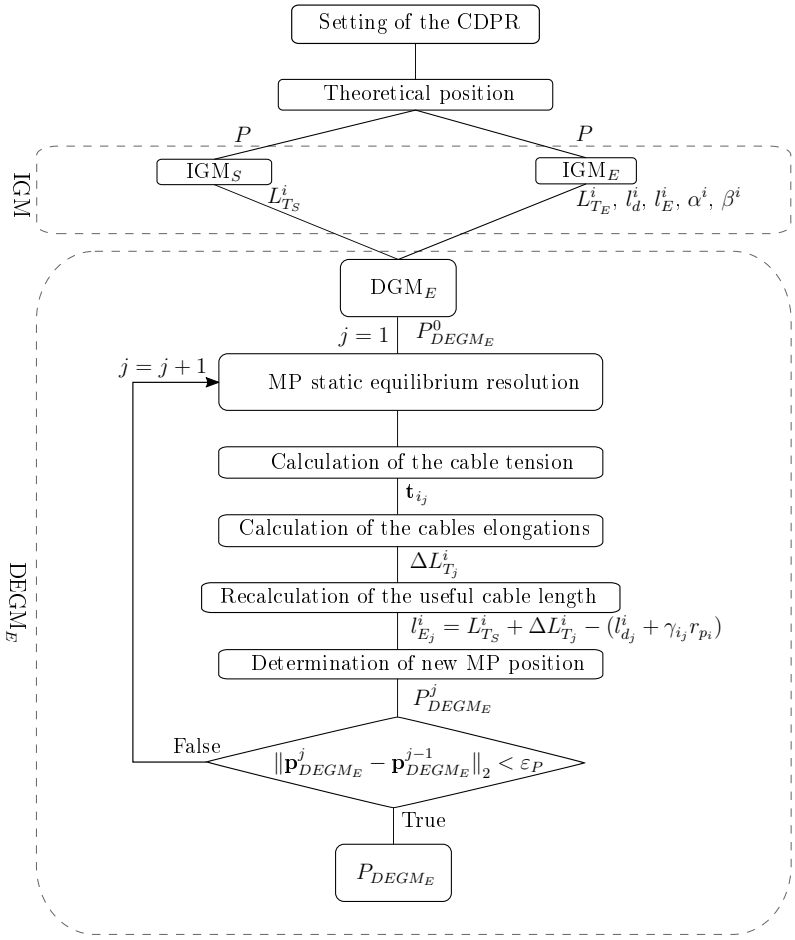

FIGURE 6 – Diagram of the resolution process of the DEGM$_E$

The following section studies the MP pose error of two suspended CDPR due to the elasto-geometrico simplifications of the IGM$_S$.

3. Moving-Platform Pose Error

The different models being established, it is then possible to evaluate and analyse the end-effector position error between the standard and the extended models. For this, after defining the evaluation position error index, different CDPR architectures are studied and presented. Finally, the MP pose errors are computed for different elasto-geometrico parameters.

3.1. Evaluation position error index

At the end of the process presented in the diagram of the Fig. 6, the positions P and P_{DEGM_E} are known. It is thus possible to determine the MP pose error $\delta\mathbf{p} = (\delta p_x \ \delta p_y \ \delta p_z)^T$ by taking into account the elasto-geometrico parameters. This error represents the difference between $\mathbf{p}_{DEGM_E}$

and the desired MP position vector $\mathbf{p}$. The index used to evaluate the position error is the norm of this difference, namely :

$$\|\delta\mathbf{p}\|_2 = \|\mathbf{p}_{MEGD_E} - \mathbf{p}\|_2 \tag{14}$$

3.2. CDPRs under study

Both studied CDPR architectures are suspended, one has three cables and the other has four cables. On the two studied CDPR the hypothesis of an MP considered like a mass point is made in order to overcome the three orientation Dof. The CDPR have only the three Dof in position, the first CDPR is said to be non-redundant because it has 3 Dof for 3 cables, the other is redundant because for the same number of Dof it has 4 cables. In addition, the values of the necessary parameters for the definition of the CDPR are fixed close to those of the CAROCA CDPR of the IRT Jules Verne [31]. The CAROCA being the subject to numerous publications [5, 32], its specifications are known. The structural dimensions are therefore fixed for the height and the sides at $5m$ for the two CDPR. Thus, the CDPR with 3 cables has a equilateral prism form (see Fig. 7a) and the CDPR with 4 cables has a cubic form (see Fig. 7b). In addition, it should be noted that in the context of this study it is supposed that the points C_i are fix and the vectors $\mathbf{a}_i$ are collinear with the $\mathbf{z}_b$ axis. The use of the winches with an exit point of the cable imposed by a guide allow to respect this hypothesis [28]. Pulleys dimensions (radius r_p and lever arm h) and cables characteristics (Young's modulus E and diameter d_c and the maximal allowed tension T_a) are summarized in Tab. 1.

Parameters	h	r_p	M	E	d_c	T_a
Values	$100mm$	$66.5mm$	$300kg$	102.2 GPa	$4mm$	$5.14kN$

TABLE 1 – Elasto-geometrico parameters of studied CDPR

Knowing the dimensions of the studied CDPR, the stopping criterion of the numerical resolution of the DEGM$_E$ is set at $\varepsilon_P = 10^{-5}m$.

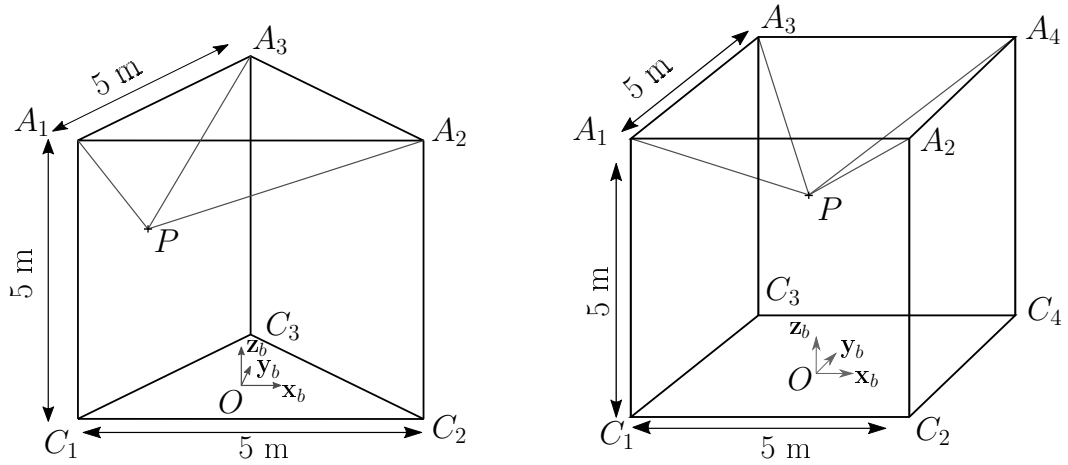

(a) CDPR3 (b) CDPR4

FIGURE 7 – Schematics drawing of the studied CDPR architectures

CDPR4 has more cables than Dof, this means that there are several possible actuation schemes to achieve the desired MP pose. Indeed, for each position in the workspace two configurations of 3 cables are solutions (see Fig. 8). For example, to position the MP at P as illustrated on Figure 8 which shown the CDPR4 in top view, the three cables configuration $A_1A_2A_3$ and $A_1A_3A_4$ are doable.

(a) Solution 1 (b) Solution 2

FIGURE 8 – Three cables among four configurations for the evaluation of the position error $\|\delta\mathbf{p}\|_2$

For each MP position, it is the lowest $\|\delta\mathbf{p}\|_2$ that chosen as the evaluation position error index of the CDPR4. For example, figure 9 shows on a horizontal plane at mid-height the workspace the distribution of the configuration that minimize $\|\delta\mathbf{p}\|_2$. This distribution turns out to be relatively different between the CDPR4$_{SR}$ et le CDPR4$_{DR}$.

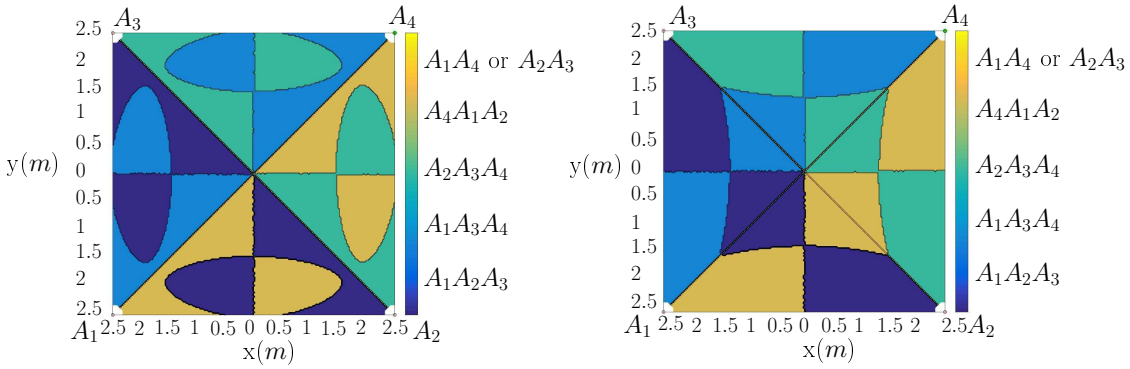

(a) CDPR4$_{SR}$ (b) CDPR4$_{DR}$

FIGURE 9 – Cable confiugrations that minimize $\|\delta\mathbf{p}\|_2$ in the horizontal plane, $z = 2.5m$

3.3. Position error analysis

This section aims to analyze the effect of pulley type and cable elasticity on the MP pose errors. First, the error on a linear trajectory through the workspace is studied, then the iso-contour of the MP pose error for a given height of the MP is presented and finally the workspace area corresponding to the MP pose error lower than a given threshold is shown. The starting point of the trajectory is $(-2.5, -1.44, 0)$ in the case of CDPR3 and $(-2.5, 0, 0)$ for CDPR4 and the end point is $(1.25, 0.72, 5)$ for CDPR3 and $(2.5, 0, 5)$ for CDPR4.

3.3.1. Position error analysis on a trajectory

The length of the path for CDPR3 and CDPR4 are $6.61m$ and $7.07m$ respectively. The position error is analysed with the evaluation index $\|\delta\mathbf{p}\|_2$. Figure 10 shows the results of $\|\delta\mathbf{p}\|_2$ for the two CDPR studied and for the two types of pulley architectures.

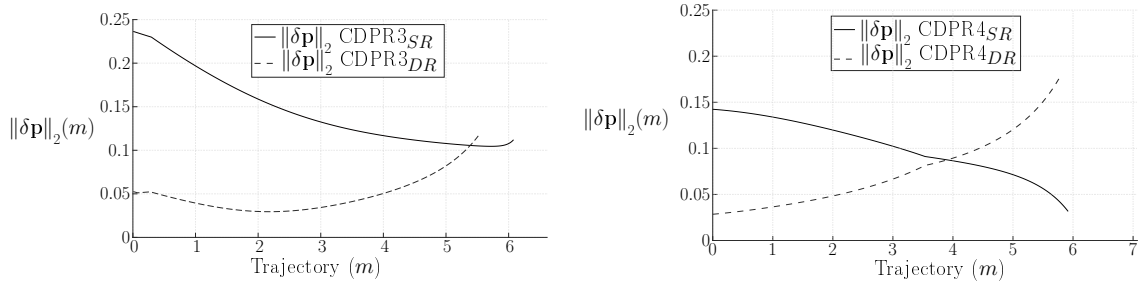

(a) CDPR3 : $\|\delta\mathbf{p}\|_2$ (b) CDPR4 : $\|\delta\mathbf{p}\|_2$

FIGURE 10 – Position errors $\|\delta\mathbf{p}\|_2$ along a linear path : $6.61m$ with 3 cables et $7.07m$ with 4 cables

First of all, it should be noted that the different errors are not evaluated until the end of the theoretical trajectories because the maximal tension in câbles is limited to T_a given in Tab. 1. For the chosen CDPR architectures, the use of single revolute joint pulley seems to allow access at a slightly greater height than double revolute joint pulleys. However, the double revolute joint pulley reduces the errors $\|\delta\mathbf{p}\|_2$ on the lower part of the trajectory. Figure 11 gives the minimum and maximum values of $\|\delta\mathbf{p}\|_2$ on the trajectory for the CDPRs under study.

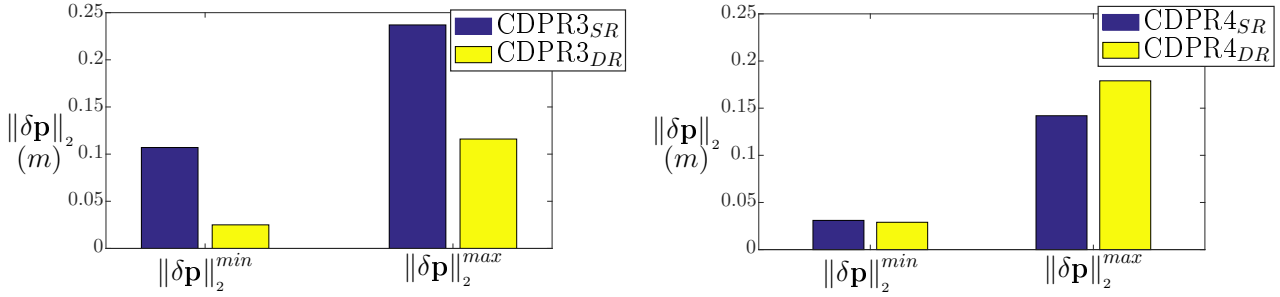

(a) CDPR3 (b) CDPR4

FIGURE 11 – Histogram of the minimum and maximum of $\|\delta\mathbf{p}\|_2$

In view of these initial results, it appears that it is difficult to neglect elasto-geometrico factors in the modelling of CDPR. Moreover, the type of pulleys has some influence on the position error $\|\delta\mathbf{p}\|_2$.

3.3.2. Position error analysis on the horizontal plane : error iso-contours

To go further in the position error analysis, the iso-contours of $\|\delta\mathbf{p}\|_2$ are plotted in a horizontal plane at mid-height of the workspace, that is, at $2.5m$. The iso-contours of Fig. 12 allow a more detailed observation of the pulleys consideration effects and the cables elasticity compared to the standard model.

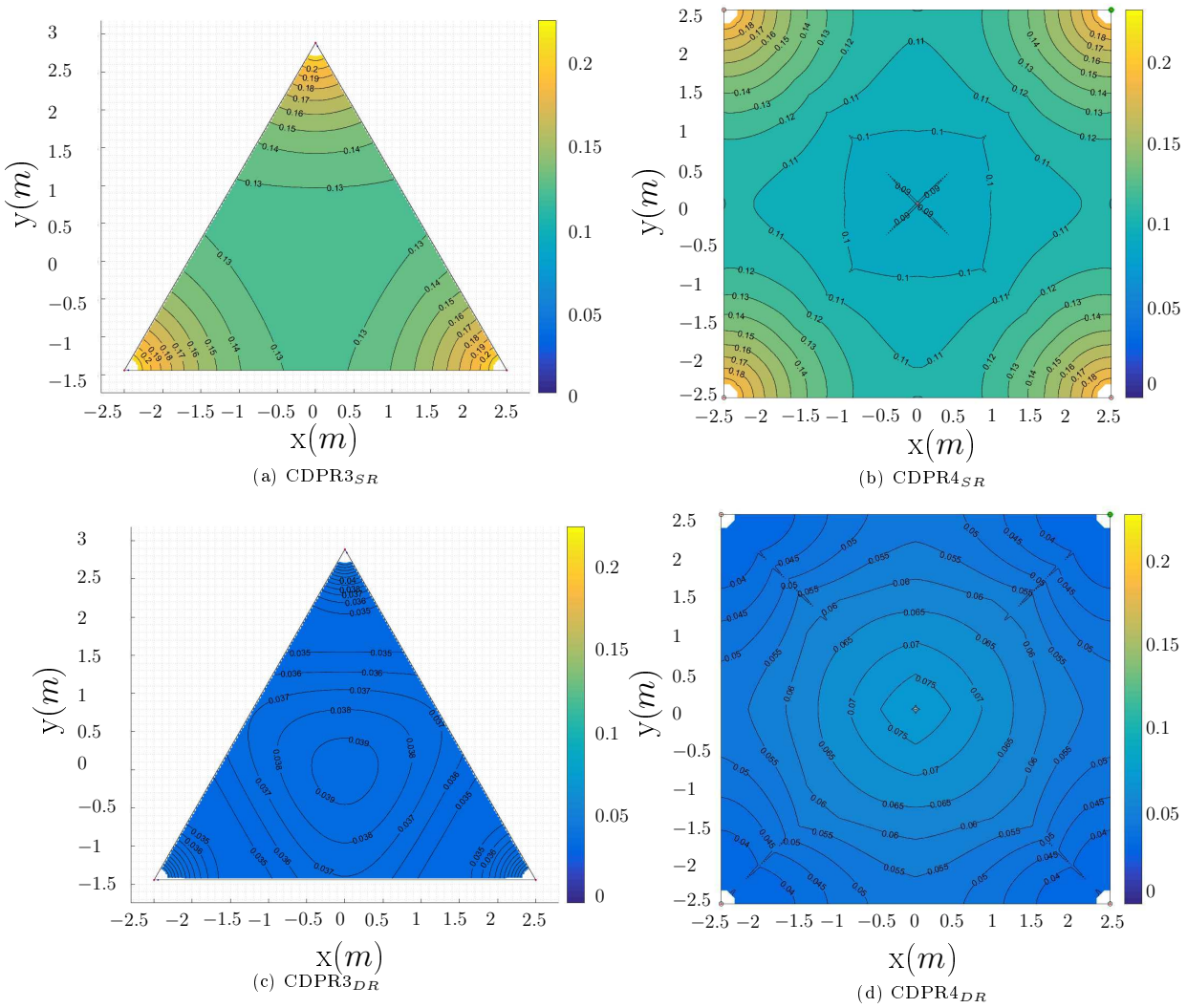

(a) CDPR3$_{SR}$ (b) CDPR4$_{SR}$

(c) CDPR3$_{DR}$ (d) CDPR4$_{DR}$

FIGURE 12 – Iso-contours of $\|\delta\mathbf{p}\|_2$ (m) throughout the horizontal plane, $z = 2.5m$

The first observation is that the iso-contours of CDPR$_{DR}$ (see Fig. 12c and Fig. 12d) always have lower values than those of the CDPR$_{SR}$ (see Fig. 12a and Fig. 12b). In addition, for the CDPR$_{SR}$, $\|\delta\mathbf{p}\|_2$ is minimal in the center of the study area ($0.13m$ for CDPR3$_{SR}$ and $0.09m$ for CDPR4$_{SR}$) and the closer the position gets to the tops of the study areas and more $\|\delta\mathbf{p}\|_2$ increases ($0.21m$ for CDPR3$_{SR}$ and $0.19m$ for CDPR4$_{SR}$). Conversely, the CDPR4$_{DR}$ has its minimum values of $\|\delta\mathbf{p}\|_2$ ($0.035m$) which are in the corners of the CDPR. For the CDPR3$_{DR}$, the minimum value of $\|\delta\mathbf{p}\|_2$ is in an intermediate area between the center and the corners. For the CDPR$_{DR}$ it is not around symmetrical positions (the MP is equidistant of the pulleys) that the position error is the smallest. It is the opposite for the CDPR4$_{DR}$ since the $\|\delta\mathbf{p}\|_2$ is maximal in the central area, with a value of $0.08m$ (see Fig. 12d). In any cases, the iso-contours of $\|\delta\mathbf{p}\|_2$ of $2.5m$ in height confirm the observation made with the trajectories, i.e. the errors are less important in the CDPR$_{DR}$ than

in the CDPR$_{SR}$.

3.3.3. Analysis of a workspace volume limited in error

The influence of the error $\|\delta\mathbf{p}\|_2$ on the CDPR workspace is now studied. To do this, the representation of an error-limited volume, noted V_L, allows to analyse the accuracy of a CDPR architecture in terms of workspace. In addition, it allows us to define the area of workspace where the $\|\delta\mathbf{p}\|_2$ is guaranteed to be less than a given error. These results are obtained by memorizing all the attainable positions in terms of maximum tension in the cables, geometric accessibility (see Eq.9) and not exceeding a limit position error noted $\|\delta\mathbf{p}\|_2^{lim}$. Then, the function *alphaShape* of Matlab® allows to generate graphically the volume V_L with a set of points and thus to determine the numerical value of this volume. To normalize the results, the ratio R_V between V_L and the total volume V_T of the CDPR outer envelope is calculated and allows to compare the four CDPR. With $V_T = 54.13m^3$ for the CDPR3 and $125m^3$ for the CDPR4. The volumes are plotted for two different $\|\delta\mathbf{p}\|_2^{lim}$ ($0.05m$ and $0.15m$). $\|\delta\mathbf{p}\|_2^{lim} = 0.05m$ is chosen because it is a "classic" position error of CDPR, that is, it correspond at $1/100$ of the outside dimensions of the CDPR, which are of $5m$. Then a maximum error three times larger is used to compare the evolution of the volumes, $\|\delta\mathbf{p}\|_2^{lim} = 0.15m$. Figure 13 shows the volumes obtained :

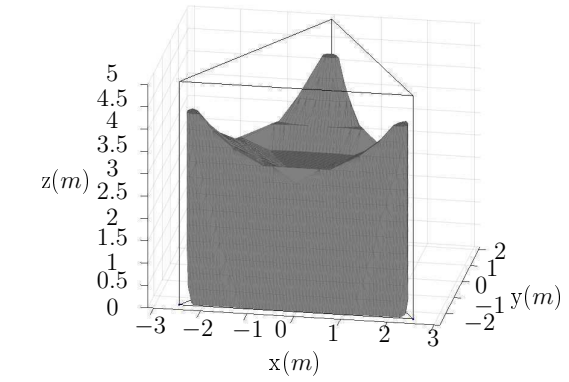

(a) CDPR3$_{DR}$ and $\|\delta\mathbf{p}\|_2^{lim} = 0.05m$: $R_V = 0.59$

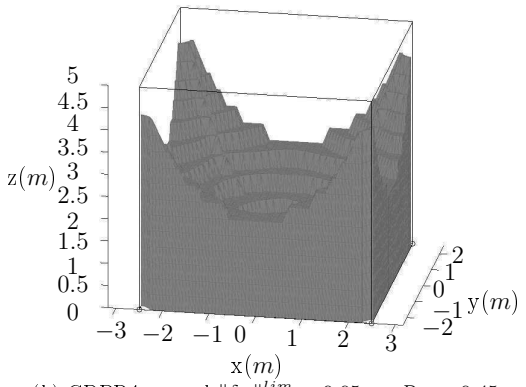

(b) CDPR4$_{DR}$ and $\|\delta\mathbf{p}\|_2^{lim} = 0.05m$: $R_V = 0.45$

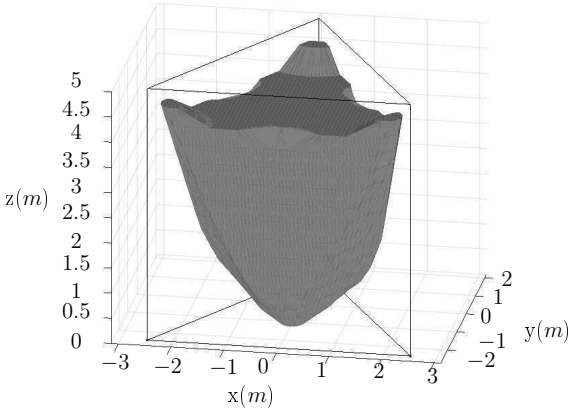

(c) CDPR3$_{SR}$ and $\|\delta\mathbf{p}\|_2^{lim} = 0.15m$: $R_V = 0.54$

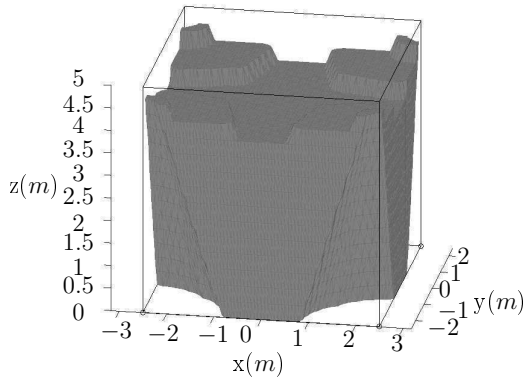

(d) CDPR4$_{SR}$ and $\|\delta\mathbf{p}\|_2^{lim} = 0.15m$: $R_V = 0.72$

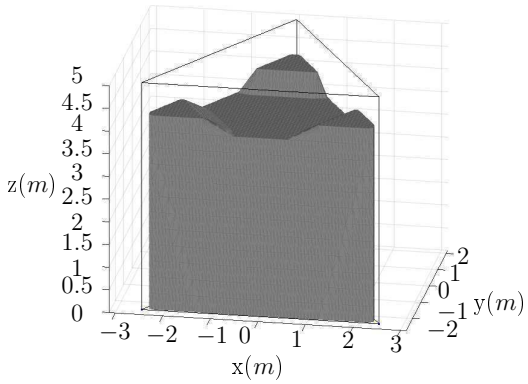

(e) CDPR3$_{DR}$ and $\|\delta\mathbf{p}\|_2^{lim} = 0.15m$: $R_V = 0.75$

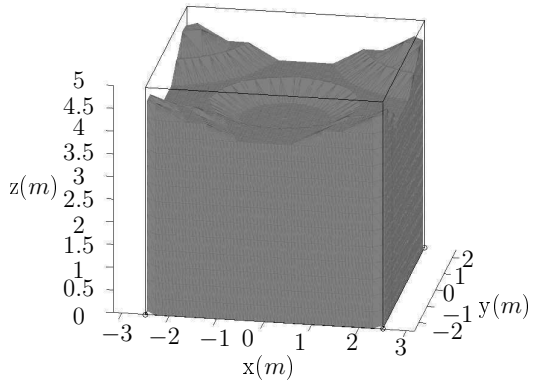

(f) CDPR4$_{DR}$ and $\|\delta\mathbf{p}\|_2^{lim} = 0.15m$: $R_V = 0.79$

FIGURE 13 – error-limited volume V_L for a $\|\delta\mathbf{p}\|_2^{lim}$

The first analyze of the limited volumes in error reveals that there are no V_L for CDPR$_{SR}$ with a $\|\delta\mathbf{p}\|_2^{lim} = 0.05m$ and thus $R_V = 0$. The second observation, in order to compare the type of

pulley, is that the R_V of the CDPR$_{DR}$ is higher than the CDPR$_{SR}$ for a same $\|\delta\mathbf{p}\|_2^{lim}$. Figure 14 shows R_V as a function of $\|\delta\mathbf{p}\|_2^{lim}$.

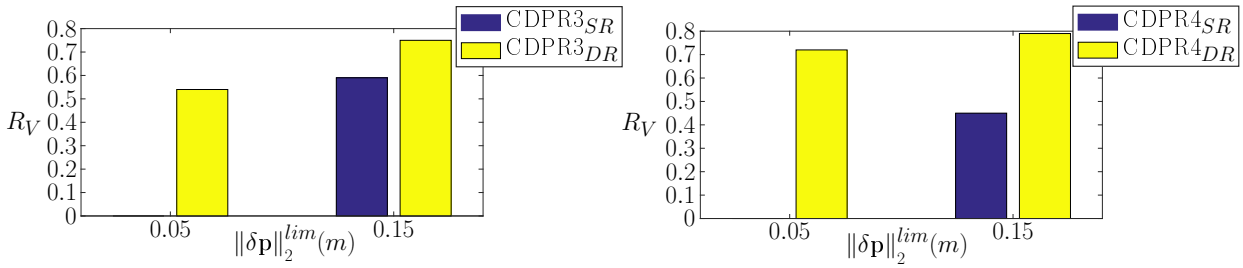

(a) R_V for CDPR3 (b) R_V for CDPR4

FIGURE 14 – Evolution of R_V as a function of $\|\delta\mathbf{p}\|_2^{lim}$ for CDPR3 and CDPR4

Moreover, Figure 13c and Figure 13d show that for the CDPR$_{SR}$ the V_L is reduced first by the workspace bottom, that is, at floor level. This can be disadvantageous as it is usually in this area that CDPR are used, for example for pick and place operations. All analyses and observations made in this section are based on a elasto-geometrico parameters fixed close to those of CAROCA. In order to analyse in a more detail led way the influence of the choice of values of the elasto-geometrico parameters (h, r_p, E and the pulley type), the next parts evaluate their effects and interactions using of the design of experiment methodology. In all cases, the proposed method allows to quantify the MP pose error for a given CDPR architecture when the cables lengths are calculated with the IGM$_S$. The choice of pulley type is important and should be considered to minimize the error when driving the CDPR with the standard geometric models. Moreover, due to the modelling made of the CDPR, the architecture with three or four cables appears to be a factor which does not significantly affect the error $\|\delta\mathbf{p}\|_2$.

4. Sensitivity of the MP error to variations in geometric parameters

The objective of this part is to determine what is the most important set of geometrical parameters on MP error, in order to guide the CDPR designers during modelling. The Young's modulus E is considered as constant ($E = 102.2$ GPa) like in part 3 and only variations of three geometrical parameters h, r_p and the pulley type on CDPR4 architectures. In this context, a comparison method of the different configurations of parameters is firstly developed. To do so, the notion of common regular workspace and a global position error evaluation index are introduced. Then, a sensitivity analysis of the geometrical parameters is carried out using a design of experiments to characterize the effects and the interactions of the geometric factors. It should be noted that the results of the design of experiment remain valid for any type of global position error evaluation index as long as it is defined from the DEGM$_E$. Finally, a research of optimal configurations of CDPR4, which minimize the position error, is presented.

4.1. Methodology for comparing different configurations of CDPR

In order to determine the most influential factors on the MP pose error, a comparison methodology must be implemented. This method is specific to the CDPR comparison and is based on the workspace size and on $\|\delta\mathbf{p}\|_2$. This method is composed of six steps :

1. Normalization of CDPR outer envelopes.

2. Calculation of DEGM_E and of $\|\delta\mathbf{p}\|_2$ of each CDPR.
3. Calculation of workspace limited on tension and in geometric accessibility.
4. Calculation of maximum regular workspace RW_{max}.
5. Research of the common regular workspace RW_C.
6. Comparison of CDPR with the use of a global position error evaluation index in the RW_C.

Concerning the first step, each CDPR must have the same footprint area as well as the same height. Steps 2 and 3 of the methodology are presented in parts 2 and 3 respectively. The workspace RW_{max} and RW_C as well as the index used in the last three steps are explained in the next two sub-sections.

4.1.1. Definition of the common regular workspace

In the CDPR, the workspace limited in tension and in geometric accessibility is rarely in regular shape (parallelepiped, cylinder, sphere, etc.), which is restrictive for the use because some areas of the workspace can be difficult to reach. In parallel robotics the concept of regular workspace RW is therefore defined to simplify the area where the manipulator can perform tasks [33]. This RW is chosen in a regular shape and is included in the workspace limited in tension and in geometric accessibility, this while maximizing its volume, hence the notion of maximum regular workspace RW_{max}. In the objective to compare the CDPR with each other, the analysis of $\|\delta\mathbf{p}\|_2$ must be done in an identical workspace for each CDPR, this space is called common regular workspace RW_C. It is determined by looking for the common intersection between all RW_{max}. In this study, since the CDPR4 outer envelopes are in parallelepiped rectangle shape, the RW_{max} are also chosen from this shape and constrained to be parallel to those of the CDPR4 outer frame. Once the RW_C of rectangular parallelepiped shape obtained, it is then possible to evaluate objectively the $\|\delta\mathbf{p}\|_2$ of each CDPR4 in view of a comparison.

4.1.2. Global position error evaluation index

The evaluation of the position errors $\|\delta\mathbf{p}\|_2$ being specific to each MP position, there is an infinite number of $\|\delta\mathbf{p}\|_2$ in the RW_C. As in part 3 it is possible to analyse the evolution of $\|\delta\mathbf{p}\|_2$ on a trajectory, on a plane or also on a volume limited in error, but this does not allow a quick comparison of CDPR. To make this comparison more generic, a global position error evaluation index must be defined. As the position error is determined for each CDPR in a common workspace, a global position error evaluation index can be chosen like a average of $\|\delta\mathbf{p}\|_2$ in the RW_C. The global position error evaluation index is then defined as follows :

$$\overline{\|\delta\mathbf{p}\|}_2 = \frac{1}{N}\sum_{i=1}^{N}\|\delta\mathbf{p}_i\|_2 \tag{15}$$

With N the number of evaluation of $\|\delta\mathbf{p}\|_2$, in these works $N = 250000$ and the positions are distributed homogeneously in the RW_C.

4.2. Sensitivity analysis of geometric parameters

It is now possible to use to analyse the sensitivity of geometric parameters with respect to $\overline{\|\delta\mathbf{p}\|}_2$. Indeed, the use of a design of experiments having as response $\overline{\|\delta\mathbf{p}\|}_2$ and as factor the geometric parameters allows to evaluate the effects and the interactions of the geometric factors on the MP

positioning error due to the use of standard models. It is important to remember that the relative comparison of the effects and the interactions observed in this part remains valid whatever the position error used, because the response of the design of experiments is based on the DEGM_E. This design of experiments therefore allows to obtain the set of influential parameters on the MP pose of the CDPR.

4.2.1. Method of analysis by design of experiment

In this part, the detailed analysis of the influence of the pulley geometric factors is realised by the design of experiments. The objective is therefore to determine the influence on $\overline{\|\delta\mathbf{p}\|_2}$ of each of the factors making up the pulley (r_p, h and type of joint). To define the minimum and maximum limits of r_p and h it is decided to oblige geometrically the pulley to conventional architecture implying that the lever arm has a dimension greater than the pulley radius, this in order to avoid possible interference between the pulley itself and its joint. To make possible the comparison, it is decided that the average of the levels of r_p is equal to the pulley radius used in part 3, i.e. $\overline{r_p} = 66.5mm$. Furthermore, to avoid fatigue or premature wear of cables, it is necessary to respect some constraints and in particular when using pulley. Indeed, a cable can be unravel if its curvature is too small, the notion of cable radius of curvature must be taken into account. In the case of pulley this radius is directly to the pulley radius r_p. Under this conditions, the usual rule is that the ratio between r_p and the cable radius r_c must be greater than 20. For certain types of cable composition (number and arrangement of strands, wires and core), this ratio may be greater or lower. In the case of the Carl Stahl Technocables Ref 1692 cable, the manufacturer indicates that the ratio between r_p and r_c must be greater than 16, that is to say :

$$\frac{r_p}{r_c} > 16 \tag{16}$$

In this study r_c is equal to $2mm$, r_p must be strictly greater than $32mm$. The low level of r_p is thus fixed at $35mm$ for safety and the high level at $98mm$. It is to highlight that the interval $r_p \in [35mm; 98mm]$ corresponds to the orders of magnitude of the pulleys radii commonly used. The limits of h are then fixed at $100mm$ for the low level and at $150mm$ for the high level to respect the constraints of geometric interferences of the pulley. The cable radius r_c is taken into account in the choice of the h limits in order to avoid the cable/revolute joint interference. The different tests of the design of experiments are presented on the table 2.

N^o	Joint	h	r_p
1	-1	-1	-1
2	-1	-1	+1
3	-1	+1	-1
4	-1	+1	+1
5	+1	-1	-1
6	+1	-1	+1
7	+1	+1	-1
8	+1	+1	+1
Field of study			
Level -1	1 revolute joint	$100mm$	$35mm$
Level +1	2 revolute joints	$150mm$	$98mm$

TABLE 2 – Full factorial design of experiments with three factors

The design of experiments is composed of eight tests. Before analysing the test results and as the eight CDPR4 configuration have a normalized outer envelopes, the RW_{max} of each CDPR4 must be determined. Among the eight RW_{max} the smallest volume is the number 6, noted RW^6_{max}. This corresponds to the configurations with the double revolute joint pulleys, $h = 100mm$ and $r_p = 98mm$. The study of the regular workspace show that the RW^6_{max} is completely included in the other seven RW_{max}, this implies that the RW^6_{max} is directly the RW_C. The volume of the RW_C, noted V_{RW_C}, is therefore $80.31m^3$.

4.2.2. Test results of the design of experiments

Knowing the RW_C, it is therefore possible to evaluate the response $\overline{\|\delta\mathbf{p}\|}_2$ for the eight tests. Figure 15 shows the results of the design of experiments in the form of histograms.

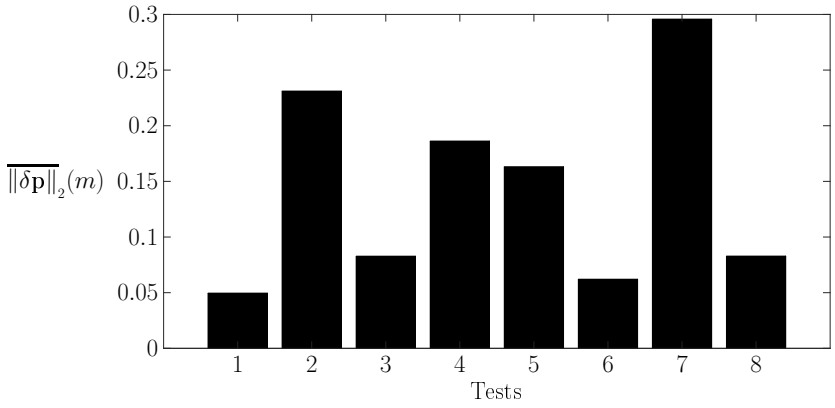

FIGURE 15 – Histograms of the responses $\overline{\|\delta\mathbf{p}\|}_2$ according to the eight tests of the design of experiments

Taking all eight tests globally, the configuration 1 minimizes the $\overline{\|\delta\mathbf{p}\|}_2$ which is worth here $0.05m$. Inversely, it is the configuration 7 which maximizes the response for a $\overline{\|\delta\mathbf{p}\|}_2$ value of $0.29m$.

Depending on the choice of geometric parameters there can be a difference of more than $0.24m$ on the average error in the RW_C. Furthermore, the tests can be differentiated in two groups, the CDPR4$_{SR}$ and the CDPR4$_{DR}$. There are the configuration 1 and 6 which minimize the most $\overline{\|\delta\mathbf{p}\|}_2$. It is observable that between the tests 1 and 3 of the CDPR4$_{SR}$ and the tests 6 and 8 of the CDPR4$_{DR}$ only the factor h changes level, but in each cases they imply a lowest variation. On the other hand, the test 2 gives the worst configuration for CDPR4$_{SR}$, but the level of factors h and r_p is identical to the test 6 ($h : -1$, $r_p : +1$) corresponding to the better level of the CDPR4$_{DR}$. These initial observations show that there appears to be a significant interaction between the three factors h, r_p and the joint type of pulley. Indeed, to improve the average error $\overline{\|\delta\mathbf{p}\|}_2$, the joint type of the pulley strongly influences the choice of the values of the geometric parameters h and r_p. The following part analyses on the whole design of experiments, the effects and the interactions between the three geometric factors.

4.2.3. Effects and interactions of geometric factors

The responses $\overline{\|\delta\mathbf{p}\|}_2$ of the tests are previously analysed, however the effects of the factors evolution remain difficult to observe overall. To do this, the design of experiment analysis method makes it possible to write a system of equations linking the results of each tests with the effects and interactions of each factor. It is then obtained the effect of each factor as well as the interactions between them according to the $\overline{\|\delta\mathbf{p}\|}_2$ criterion evaluated in the RW_C. Figure 16 shows the effects and interactions between parameters in the form of a histogram.

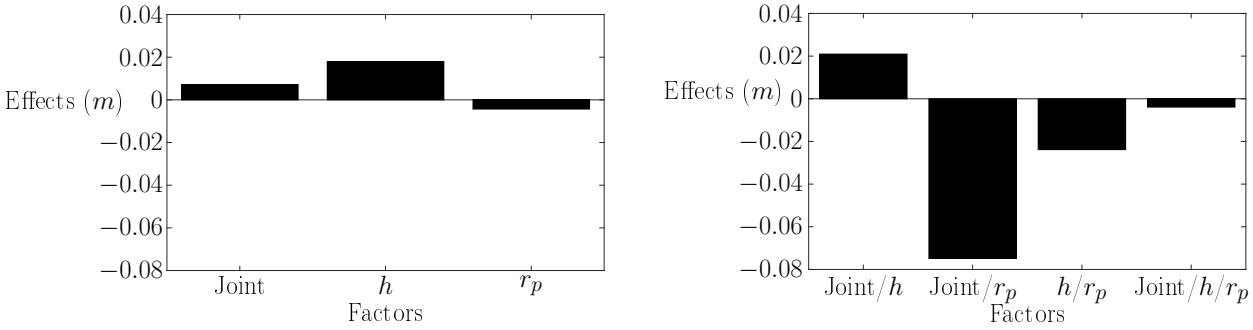

(a) Parameter effects

(b) Interactions between the parameters

FIGURE 16 – Effects and interactions of the different factors on $\overline{\|\delta\mathbf{p}\|}_2$

This results confirm the first observations made in part 4.2.2. Indeed, it is notable that the interaction between the pulley radius r_p and the joint type plays a major role in the evolution of $\overline{\|\delta\mathbf{p}\|}_2$ and that the interaction between h and the joint type of the pulley cannot be neglected. In addition, the effect of the joint alone does not appear to be significant. However, in view of the interaction with the other factors, it implies that the choice of the joint has an impact on $\overline{\|\delta\mathbf{p}\|}_2$. This confirms the need to pay attention to the coupling of geometric factors resulting from the presence of pulleys. It is also noteworthy that in the future works, the interaction of the third order being relatively weak in view of the results obtained, it could initially be neglected. When choosing the pulley architecture the designer cannot neglect any of the effects and second order interactions of the three studied geometric parameters. In addition, to conserve the use of the standard models there must be a geometric configuration of h and r_p for each pulley type (single or double revolute

joints) which minimizes $\overline{\|\delta\mathbf{p}\|}_2$. The following part search the configurations, which optimise the position error.

4.3. Search for configurations which optimize the position error

The previous observations show that to minimize $\overline{\|\delta\mathbf{p}\|}_2$, the couple of geometric parameters h and r_p does not behave in the same way depending on the number of pulley revolute joints. To illustrate this difference of behaviour, the number of parameters being of two, it is possible to plot a iso-contours of $\overline{\|\delta\mathbf{p}\|}_2$ in the RW_C according to h and r_p for each pulley type. These iso-contours allow to determine optimal configurations of CDPR4$_{SR}$ and CDPR4$_{DR}$ according to $\overline{\|\delta\mathbf{p}\|}_2$. Figure 17 show as an iso-contours the change in the average position error according to h and r_p. In addition, the study field of the design of experiments, limited by the low and high level of the factors h and r_p is represented on Fig. 17a and Fig. 17b by the points T_i $(i = 1, \ldots, 8)$ representing the tests 1, 2, 3 and 4 respectively for the CDPR4$_{SR}$ and the tests 5, 6, 7 and 8 for the CDPR4$_{DR}$. The placement of T_i points on the iso-contours of $\overline{\|\delta\mathbf{p}\|}_2$ allow to better illustrate the results of the design of experiments (see Fig. 15). It should also be noted that the analyse is reduced to a triangle shape because the pulleys are geometrically constrained so that the lever arm h has a dimension greater than the pulley radius r_p to avoid the interference.

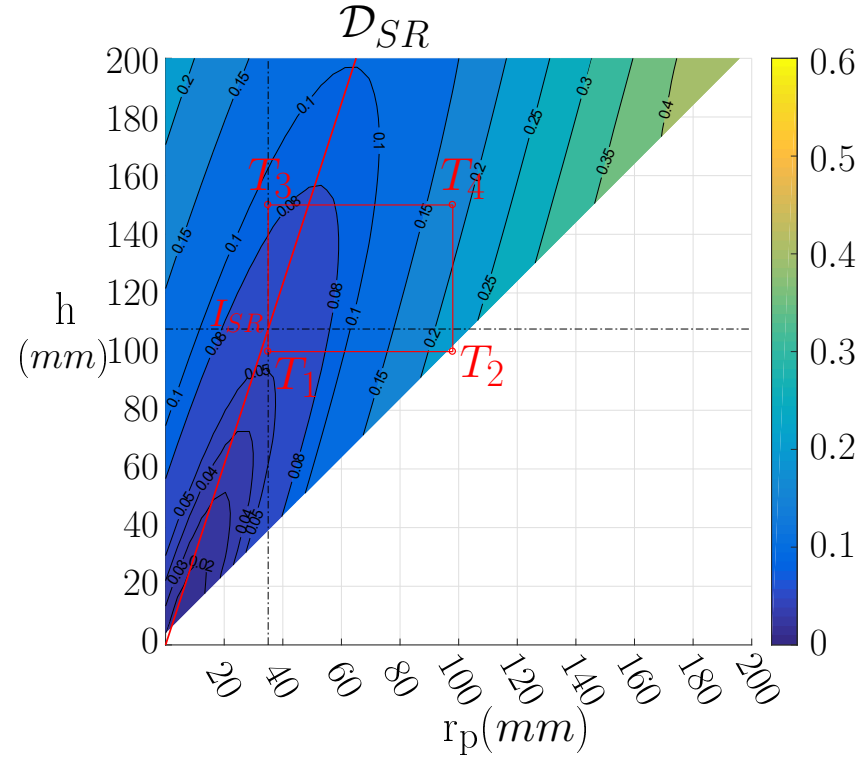

(a) CDPR4$_{SR}$

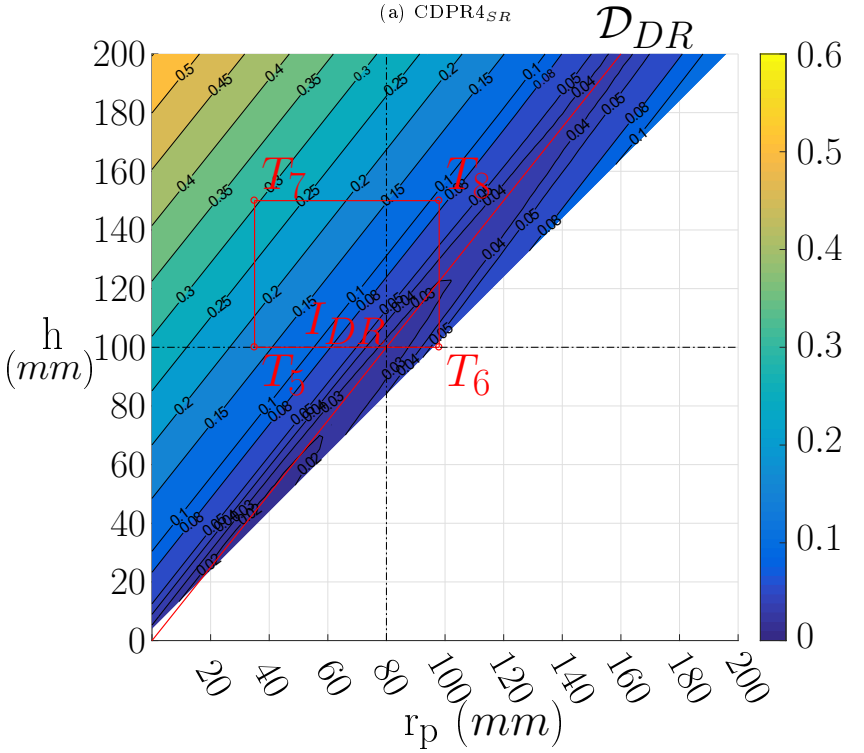

(b) CDPR4$_{DR}$

FIGURE 17 – Average of the position errors $\overline{\|\delta\mathbf{p}\|_2}$ in m according to the pulley radius r_p and this lever arm h

The iso-contours of Fig. 17a and Fig. 17b clearly show different areas which minimize $\overline{\|\delta\mathbf{p}\|}_2$ between the CDPR4$_{SR}$ and the CDPR4$_{DR}$. However, the error $\overline{\|\delta\mathbf{p}\|}_2$ is minimal if $h = r_p = 0mm$ because this corresponds to the setting of standard models. It is then possible to find the equations of lines $\mathcal{D}_{SR}$ et $\mathcal{D}_{DR}$, respectively for CDPR4$_{SR}$ and CDPR4$_{DR}$, which pass through the origin and which give the linear relation between the h and the r_p which minimize $\overline{\|\delta\mathbf{p}\|}_2$. The resulting equations are the following :

$$\mathcal{D}_{SP} : h = \frac{40}{13} r_p \tag{17}$$

$$\mathcal{D}_{DP} : h = \frac{5}{4} r_p \tag{18}$$

For a given value of h or r_p these equations allow to determine the set of parameters (h,r_p) which minimizes $\overline{\|\delta\mathbf{p}\|}_2$. The results of Fig. 17a and Fig. 17b also indicate that the closer the set of parameters (h,r_p) is to the origin (0,0), the lower is $\overline{\|\delta\mathbf{p}\|}_2$. In these conditions and with the parameters h and r_p limited their high and low levels, it appears that the intersections I_{SR} and I_{DR} (see Fig. 17) of the lines $\mathcal{D}_{SR}$ and $\mathcal{D}_{DR}$ with the study field of the design of experiments, correspond to the optimal configurations of h and r_p which minimize $\overline{\|\delta\mathbf{p}\|}_2$. The results of geometric parameters for the optimal architectures noted CDPR4$_{SR}{}^*$ et CDPR4$_{DR}{}^*$ are summarized in the Tab. 3.

Architectures	CDPR4$_{SR}{}^*$	CDPR4$_{DR}{}^*$
h	$107.7mm$	$100mm$
r_p	$35mm$	$80mm$
$\overline{\|\delta\mathbf{p}\|}_2$	$53.75mm$	$23.28mm$

TABLE 3 – Values of optimal geometric parameters h and r_p which minimize $\overline{\|\delta\mathbf{p}\|}_2$ in the studied design of experiments

Thus, the CDPR4$_{DR}$ has a configuration that minimizes the most $\overline{\|\delta\mathbf{p}\|}_2$ in the limited study field by the design of experiments. Furthermore, the slope of the line $\mathcal{D}_{DR}$ is lower than that of $\mathcal{D}_{SR}$, this implies that it is possible to significantly increase r_p while keeping a relatively low $\overline{\|\delta\mathbf{p}\|}_2$. Knowing the constraints of the maximum bending radius of the cables, if r_p increases then the cable diameter can increase and thus the transportable mass as well. The CDPR4$_{DR}$ appears to be better able to carry heavy loads when the designer wants to minimize the MP pose error made by using the standard models. With all of the results obtained in this part, the use of the double revolute joints pulley in the suspended CDPR4 minimizes generally the MP pose error between the standard and extended models. However, [27] shows that the Young's modulus E of cables has a high variation during its use caused by a non-linear behaviour as a function of the tension in the cable and a hysteresis phenomenon between the loading and the unloading. Therefore, depending on the use of CDPR, there is an uncertainty about the study [27] and thus on the index $\overline{\|\delta\mathbf{p}\|}_2$. The following part quantifies this uncertainty for the two optimal configurations CDPR4$_{SR}{}^*$ et CDPR4$_{DR}{}^*$.

5. Effect of cable elasticity to the MP pose error

The influence of the geometric parameters composing the two pulley architectures is analysed in the previous part. However, the elastic behaviour of cables is a factor that can significantly influence

the end-effector pose error of the CDPR, as shown in numerous studies [17, 27, 34]. The study carried out so far considers the elasticity in the cables as constant and equal at 102.2 GPa for the Young's modulus E. It is now interesting to study the influence of its variation on the end-effector global position error evaluation index. Many factors can cause a cable to have a variable E during its use. Indeed, due to its design, a cable presents a relatively important hysteresis phenomenon of the elasticity between its loading and unloading [35]. Moreover, [36], highlights a non-linears evolution of E during the tension variation in the cable and [27] shows that the uncertainly on E allow be up to tens of GPa. According to cable manufacturers, the Young's modulus can also vary with the age of cables, especially during the first hours of use when the strands find their equilibrium position in the cables. First in this part, the uncertainly on $\overline{\|\delta\mathbf{p}\|}_2$ in the RW_C due to the variability of E is quantified for the optimal configurations. Then, the uncertainty evolution of $\|\delta\mathbf{p}\|_2$ of CDPR4$_{SR}{}^*$ and of CDPR4$_{DR}{}^*$ on a trajectory is analysed to complete the study.

5.1. Quantification of the uncertainty on the global position error evaluation index

To study the influence of the variability of Young's modulus E, the analyse is based on the variation of $\overline{\|\delta\mathbf{p}\|}_2$ in RW_C according to the evolution of E. It should be remembered that according to ISO 12076, a cable must work between 10% and 30% of its breaking load T_r. However, as mentioned in [27], a cable installed on a CDPR does not necessarily work in this interval. In these works, it is considered that the cables work between 5% and 50% of T_r. Considering the experimental results presented in the Baklouti's article [27] and by extrapolating the values of E, an uncertainty of 70 GPa equally distributed around 102.2 GPa is determined. This incertitude ± 35 GPa allow to cover the whole range of variation of the elasticity (hysteresis, % of tensions, cable aging). The elasticity modulus is then restricted to the interval [67.2 GPa; 137.2 GPa] because $E = 102.2 \pm 35$ GPa. Figure 18 represents the evolution of $\overline{\|\delta\mathbf{p}\|}_2$ according to the Young's modulus E of cable and this for each optimal configurations determined previously, i.e. for the CDPR4$_{SR}{}^*$ et le CDPR4$_{DR}{}^*$.

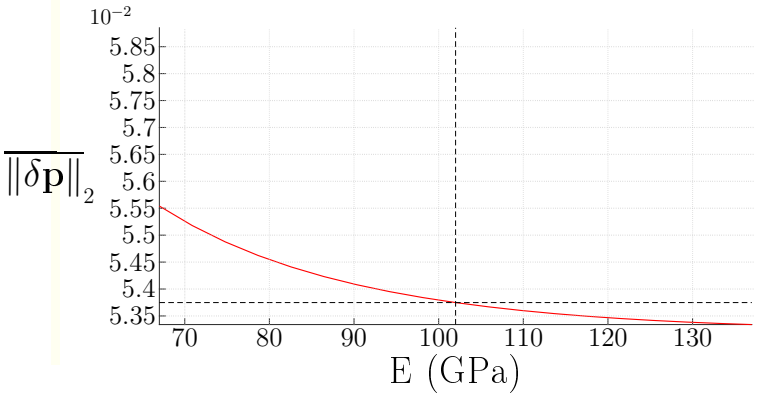

(a) CDPR4$_{SR}{}^*$

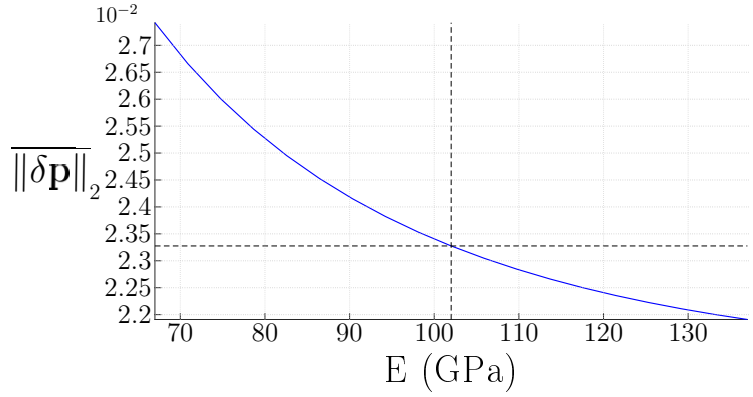

(b) CDPR4$_{DR}{}^*$

FIGURE 18 – Uncertainty on $\overline{\|\delta\mathbf{p}\|}_2$ in m due to a variation of $E = 102.2 \pm 35$ GPa

It is then possible to determine that the average of the errors included in the RW_C is $\overline{\|\delta\mathbf{p}\|}_2 = 53.75^{+1.5}_{-0.29} mm$ for the CDPR4$_{SR}{}^*$ and $\overline{\|\delta\mathbf{p}\|}_2 = 23.28^{+3.9}_{-1.2} mm$ for the CDPR4$_{DR}{}^*$. The total variation $\Delta\overline{\|\delta\mathbf{p}\|}_2$ of $1.79mm$ for the CDPR4$_{SR}{}^*$ represents 3.33% of the mean error for a $E = 102.2$ GPa. In the case of CDPR4$_{DR}{}^*$ a total uncertainty of $\Delta\overline{\|\delta\mathbf{p}\|}_2 = 5.1mm$ represents 21.91%. With these results, it is possible to say that the optimal configuration CDPR4$_{SR}{}^*$ has an average position error in RW_C more robust than that of CDPR4$_{DR}{}^*$ against variations in the elasticity of the cables. Finally, even if the $\overline{\|\delta\mathbf{p}\|}_2$ of CDPR4$_{SR}{}^*$ is less sensitive to the variation of E, this minimal values which is of $53.46mm$ remains much higher than the maximum value of $\overline{\|\delta\mathbf{p}\|}_2$ of CDPR4$_{DR}{}^*$ which is of $27.18mm$. The following part analyses the evolution of the uncertainty of $\|\delta\mathbf{p}\|_2$ on a rectilinear trajectory through the RW_C.

5.2. Uncertainty evolution of the position error on a trajectory

To observe in detail the effect of the variation of the Young's modulus of cables on a uncertainty of $\|\delta\mathbf{p}\|_2$ of the CDPR4$_{SR}{}^*$ and of the CDPR4$_{DR}{}^*$, the evolution of $\|\delta\mathbf{p}\|_2$ along a rectilinear trajectory through the RW_C is plotted for three different elasticities. This trajectory has as starting point $(-2.32, 0, 0)$ and as end-point $(2.32, 0, 3.75)$. The evolution of $\|\delta\mathbf{p}\|_2$ along this theoretical

trajectory is plotted for $E_{min} = 67.2$ GPa, $E_{mean} = 102.2$ GPa and $E_{max} = 137.2$ GPa. Figure 19 illustrates the results obtained.

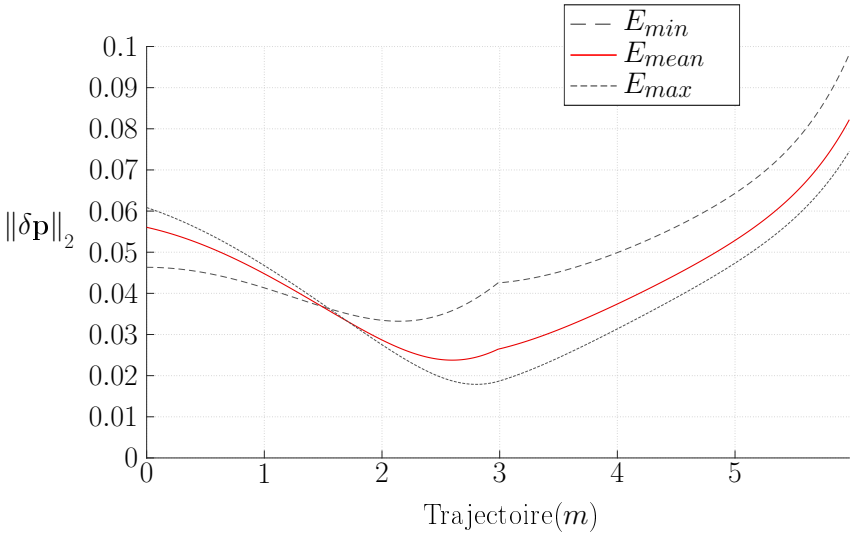

(a) CDPR4$_{SR}{}^*$

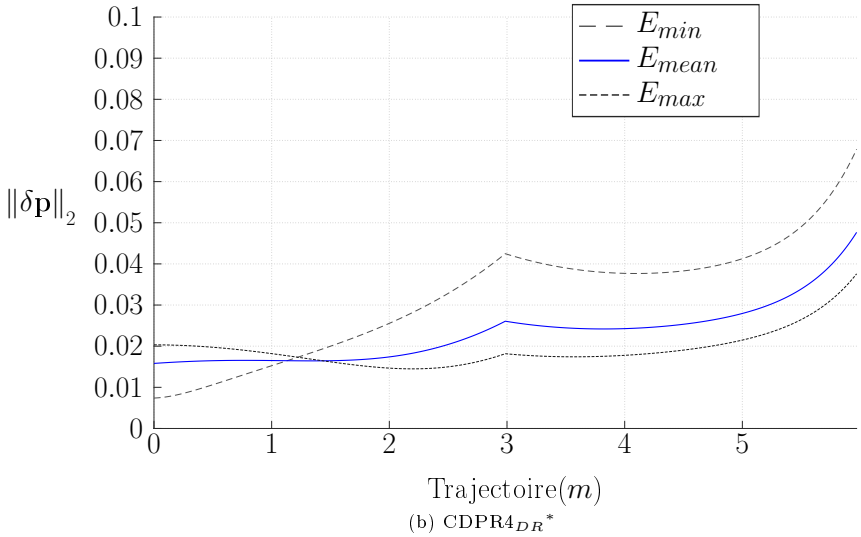

(b) CDPR4$_{DR}{}^*$

FIGURE 19 – Evolution of $\|\delta \mathbf{p}\|_2$ along a given path for E_{min}, E_{mean} et E_{max}

The following notations are used in the rest of the study : $\|\delta \mathbf{p}\|_2^{E_k}$ with $k = [min, mean, max]$ according to that the $\|\delta \mathbf{p}\|_2$ is evaluated with E_{min}, E_{mean} or E_{max} on all cables. First of all, what is interesting to note is that at the bottom of the RW_C, it is the position error $\|\delta \mathbf{p}\|_2^{E_{max}}$ which are the most important. It is therefore not always for the greatest Young's modul of the cables that the position error is smallest. An inversion between $\|\delta \mathbf{p}\|_2^{E_{max}}$ and $\|\delta \mathbf{p}\|_2^{E_{min}}$ occurs at a postion of $1.55m$ along the trajectory for the CDPR4$_{SR}{}^*$ and of $1.23m$ for the CDPR4$_{DR}{}^*$. It is therefore above these positions that the configurations with elasticity E_{max} on the cables minimize $\|\delta \mathbf{p}\|_2$. In addition, for the same E the CDPR4$_{SR}{}^*$ has always a higher position error than the CDPR4$_{DR}{}^*$.

This observation is consistent with the results of $\overline{\|\delta\mathbf{p}\|}_2$ illustrated on Fig. 18. Furthermore, it appears that the uncertainty on the $\|\delta\mathbf{p}\|_2$ of the CDPR4$_{DR}{}^*$ are in generally higher than those of the CDPR4$_{SR}{}^*$. This observation is mainly found on the second half of the trajectory, at a position above $3m$. It should be noted that the abrupt change in curvature at this position corresponds to a change in configuration of 3 cables among the 4 cables available CDPR4. Analyzing the obtained results, it is clear that for a CDPR, the variation of Young's modulus which can appear during the use of the cable as well as during whole of its life, plays a not negligible role on the MP pose error of the CDPR. The uncertainty caused by this modification of the mechanical characteristics of cables does not translate identically according to the pulley types chosen. The CDPR4 equiped with pulley being a single revolute joint is more robust to the variations in cable elasticity than the CDPR4 with double revolute joint. However, the uncertainty on the MP global position error evaluation index does not change the fact that the architecture that minimizes the most $\|\delta\mathbf{p}\|_2$ remains the CDPR4$_{DR}{}^*$.

Conclusion

This paper dealt with the modeling of cable-driven parallel robots (CDPRs) while considering pulley kinematics and cable elasticity. The extended elasto-geometrico static models are used to analyse the MP pose error in regards to standard geometric static models frequently used in the literature. Then, the influence of variations in geometric parameters on the pose error of two types of pulley architectures is quantified. A method is then proposed to obtain numerically the solution of extended direct elasto-geometrico static model. Moreover, once the CDPR studied is redundant a method is proposed to choose the configuration of three cables among four minimizing the MP pose errors. Furthermore, a comparison methodology of CDPRs architectures is established and serves for sensitivity analysis. Besides, two types of pulley architectures were investigated, one classical and one innovant pulley. The CDPR equipped with the novel pulley minimizes the MP pose error in most of the Cartesian workspace. Results also state on the necessity to take into account the geometrical parameters of the pulleys during the modelling of the CDPRs. Furthermore, the observation of behaviour of the global position error evaluation index as a function of the pulley radius and its lever arm shows a significant difference between the two types of pulleys, indeed the global positioning error of the end-effector is equal to $\overline{\|\delta\mathbf{p}\|}_2 = 23.28mm$ for CDPR4$_{DR}{}^*$ while for CDPR4$_{SR}{}^*$ $\overline{\|\delta\mathbf{p}\|}_2 = 53.75mm$. The optimal configurations of CDPRs, as a function of the pulley type to minimize the MP pose error has been determined. The choice of pulleys has been demonstrated to play an important role on the accuracy and robustness of the final design of CDPRs. In addition, the novel double revolute joint pulleys seems to be promising for use in the CDPRs field. Indeed, it increases the R_V and its efficienty in view of $\overline{\|\delta\mathbf{p}\|}_2$. Later on, due to the influence of uncertainty of cables Young's modulus on the accuracy of CDPRs, a more in-depth study dealing with the variations in cable elasticity will be carried out since the real value of each of Young's modulus differs from one cable to another due to the history of loading and unloading previous sequences.

List of Abbreviations

α_i	Angle respect the static equilibrium of CDPR
β_i	Angle between the horizontal plane $(O, \mathbf{x}_b, \mathbf{y}_b)$ and $\mathbf{h}_i$
ϵ_p	Stop criterion
γ_i	Angle between $\mathbf{d}_i$ and $\mathbf{k}_i$

$\mathcal{F}_b$	General base frame
$\mathcal{F}_p$	Base frame of MP
ϕ_i	Angle between $\mathbf{a}_i$ and $\mathbf{l}_S^i$
$\mathbf{a}_i$	Vector between A_i and C_i
$\mathbf{b}_i$	Vector between P and B_i
$\mathbf{c}_i$	Vector between O and C_i
$\mathbf{d}_i$	Vector between H_i and D_i
$\mathbf{l}_d^i$	Vector of dead length of i^{th} cable
$\mathbf{l}_E^i$	Vector of extended useful length of i^{th} cable
$\mathbf{l}_S^i$	Vector of standard useful length of i^{th} cable
$\mathbf{M}$	Square matrix
$\mathbf{p}$	Vector between O and P
$\mathbf{R}$	Rotation matrix between $\mathcal{F}_b$ and $\mathcal{F}_p$
$\mathbf{t}$	Vector of cables tensions
$\mathbf{t}_{di}$	Tension in the dead length of i^{th} cable
$\mathbf{t}_u$	Tension in the useful length of i^{th} cable
$\mathbf{W}$	Wrench matrix
$\mathbf{w}_{ext}$	External wrench applied to the MP
θ_i	Angle between x_{pul} and $\mathbf{d}_i$
A_i	i^{th} Cable exit point
B_i	i^{th} Cable anchor point
C_i	i^{th} Cable exit point of the winch
D_i	Exit point of the i^{th} pulley
H_i	Center of i^{th} pulley
h_i	Lever arm of i^{th} cable
K_i	Enter point of the i^{th} pulley
l_d^i	Length dead of i^{th} cable
l_E^i	Extended useful length of i^{th} cable
l_S^i	Standard useful length of i^{th} cable
L_{TE}^i	Total extended length of i^{th} cable
L_{TS}^i	Total standard length of i^{th} cable
m	Number of cable
n	Number of DDLs
r_{pi}	Radius of i^{th} cable
CDPR	Cable-Driven Parallel Robot
CDPR_{DR}	CDPR with double revolute joint pulley
CDPR_{SR}	CDPR with single revolute joint pulley
CDPR3	CDPR with three cables
CDPR4	CDPR with four cables
DEGM_E	Extended Direct Elasto-Geometrico Model
DGM	Direct Geometric static Models
DGM_E	Extended Direct Geometric static Models
IGM	Inverse Geometric static Models
IGM_S	Standard Inverse Geometric static Models
MP	Moving-Platform

Références

[1] J.-P. Merlet, Parallel Robots Second Edition, Springer-Verlag New York Inc., 2006.

[2] A. Pashkevich, P. Wenger, D. Chablat, Design strategies for the geometric synthesis of orthoglide-type mechanisms, Mechanism and Machine Theory 40 (8) (2005) 907–930.
URL https://doi.org/10.1016/j.mechmachtheory.2004.12.006

[3] M. Stock, K. Miller, Optimal kinematic design of spatial parallel manipulators : Application to linear delta robot, Journal of Mechanical Design 125 (2) (2003) 292–301.
URL https://doi.org/10.1115/1.1563632

[4] B. Duan, A new design project of the line feed structure for large spherical radio telescope and its nonlinear dynamic analysis, Mechatronics 9 (1) (1999) 53–64.
URL https://doi.org/10.1016/S0957-4158(98)00028-2

[5] L. Gagliardini, S. Caro, M. Gouttefarde, A. Girin, Discrete reconfiguration planning for cable-driven parallel robots, Mechanism and Machine Theory 100 (2016) 313–337.
URL https://doi.org/10.1016/j.mechmachtheory.2016.02.014
[6] S. Qian, B. Zi, W.-W. Shang, Q. Xu, A review on cable-driven parallel robots, Chinese Journal of Mechanical Engineering 31 (1) (2018) 66.
URL https://doi.org/10.1186/s10033-018-0267-9
[7] F. Liu, W. Xu, H. Huang, Y. Ning, B. Li, Design and analysis of a high-payload manipulator based on a cable-driven serial-parallel mechanism, Journal of Mechanisms Robotics 11 (2) (2019) 290–295.
URL https://doi.org/10.1115/1.4044113
[8] L. Gagliardini, S. Caro, M. Gouttefarde, A. Girin, A reconfiguration strategy for reconfigurable cable-driven parallel robots, in : 2015 IEEE International Conference on Robotics and Automation (ICRA), 2015, pp. 1613–1620.
URL https://doi.org/10.1109/ICRA.2015.7139404
[9] J.-B. Izard, A. Dubor, P.-E. Hervé, E. Cabay, D. Culla, M. Rodriguez, M. Barrado, On the improvements of a cable-driven parallel robot for achieving additive manufacturing for construction, in : Cable-Driven Parallel Robots. Mechanisms and Machine Science, Vol. 53, 2018.
URL https://doi.org/10.1007/978-3-319-61431-1_30
[10] R. Thompson, M. Blackstone, Three-Dimensional Moving Camera Assembly with an Informational Cover Housing, United States Patent no. US6873355, 2005.
[11] G. Meunier, B. Boulet, M. Nahon, Control of an overactuated cable-driven parallel mechanism for a radio telescope application, IEEE Transactions on Control Systems Technology 17 (5) (2009) 1043–1054.
URL https://doi.org/10.1109/TCST.2008.2004812
[12] J.-P. Merlet, Some properties of the irvine cable model and their use for the kinematic analysis of cable-driven parallel robots, Mechanism and Machine Theory 135 (2019) 271–280.
URL https://doi.org/10.1016/j.mechmachtheory.2019.02.009
[13] G. Barrette, C. Gosselin, Determination of the dynamic workspace of cable-driven planar parallel mechanisms, Journal of Mechanical Design 127 (2) (2005) 242–248.
URL https://doi.org/10.1115/1.1830045
[14] G. Abbasnejad, M. Carricato, Real solutions of the direct geometrico-static problem of under-constrained cable-driven parallel robots with 3 cables : a numerical investigation, Meccanica 47 (2012) 1761–1773.
URL https://doi.org/10.1007/s11012-012-9552-3
[15] A.-B. Alp, S. Agrawal, Cable suspended robots : design, planning and control, in : Proceedings 2002 IEEE International Conference on Robotics and Automation, Vol. 4, 2002, pp. 4275–4280.
URL https://doi.org/10.1109/ROBOT.2002.1014428
[16] L. Gagliardini, S. Caro, M. Gouttefarde, P. Wenger, A. Girin, A reconfigurable cable-driven parallel robot for sand-blasting and painting of large structures, in : Cable-Driven Parallel Robots. Mechanisms and Machine Science, Vol. 32, 2015.
URL https://doi.org/10.1007/978-3-319-09489-2_20
[17] D. Nguyen, M. Gouttefarde, O. Company, F. Pierrot, On the simplifications of cable model in static analysis of large-dimension cable-driven parallel robots, in : 2013 IEEE/RSJ International Conference on Intelligent Robots and Systems, 2013, pp. 928–934.
URL https://doi.org/10.1109/IROS.2013.6696461
[18] H. Yuan, E. Courteille, D. Deblaise, Static and dynamic stiffness analyses of cable-driven parallelrobots with non-negligible cable mass and elasticity, Mechanism and Machine Theory 85 (2015) 64–81.
URL https://doi.org/10.1016/j.mechmachtheory.2014.10.010
[19] X. Weber, L. Cuvillon, J. Gangloff, Active vibration canceling of a cable-driven parallel robot in modal space, in : 2015 IEEE International Conference on Robotics and Automation (ICRA), 2015, pp. 1599–1604.
URL https://doi.org/10.1109/ICRA.2015.7139402
[20] G. Abbasnejad, M. Carricato, Direct geometrico-static problem of underconstrained cable-driven parallel robots with n cables, IEEE Transactions on Robotics 31 (2) (2015) 468–478.
URL https://doi.org/10.1109/TRO.2015.2393173
[21] G. Abbasnejad, M. Carricato, Real solutions of the direct geometrico-static problem of under-constrained cable-driven parallel robots with 3 cables : a numerical investigation, Meccanica 47 (7) (2012) 1761–1773.
URL https://doi.org/10.1007/s11012-012-9552-3
[22] X. Jin, J. Jung, J. Piao, E. Choi, J. Park, C. Kim, Solving the pulley inclusion problem for a cable-driven parallel robotic system : Extended kinematics and twin-pulley mechanism, Journal of Mechanical Science and Technology 32 (6) (2018) 2829–2838.
URL https://doi.org/10.1007/s12206-018-0539-4
[23] A. Pott, Influence of pulley kinematics on cable-driven parallel robots, Latest Advances in Robot Kinematics (2012) 197–204.
URL https://doi.org/10.1007/978-94-007-4620-6_25
[24] O. Bohigas, M. Manubens, L. Ros, Planning wrench-feasible motions for cable-driven hexapods, in : IEEE Transactions on Robotics, Vol. 32, 2016, pp. 442–451.
URL https://doi.org/10.1109/TRO.2016.2529640
[25] L. Gagliardini, S. Caro, M. Gouttefarde, P. Wenger, A. Girin, Optimal design of cable-driven parallel robots for large industrial structures, in : 2014 IEEE International Conference on Robotics and Automation (ICRA), 2014, pp. 5744–5749.
URL https://doi.org/10.1109/ICRA.2014.6907703
[26] X. Jin, J. Jung, S. Ko, E. Choi, J. Park, C. Kim, Geometric parameter calibration for a cable-driven parallel robot based on a single one-dimensional laser distance sensor measurement and experimental modeling, Sensors 18 (7) (2018)

2392.
URL https://doi.org/10.3390/s18072392
[27] S. Baklouti, S. Caro, E. Courteille, Sensitivity analysis of the elasto-geometrical model of cable-driven parallel robots 53.
URL https://doi.org/10.1007/978-3-319-61431-1_4
[28] X. Jin, J. Piao, E. Choi, J. Jung, J. Park, C. Kim, A novel winch system for a precise cable length control of a cable-driven parallel robot system, in : International Symposium on Robotics (ISR), 2017.
[29] L. Nurahmi, B. Pramujati, S. Caro, Dimension synthesis of suspended eight cables-driven parallel robot for search-and-rescue operation, in : 2017 International Conference on Advanced Mechatronics, Intelligent Manufacture, and Industrial Automation (ICAMIMIA), 2017, pp. 237–241.
URL https://doi.org/10.1109/ICAMIMIA.2017.8387594
[30] R. Roberts, T. Graham, T. Lippitt, On the inverse kinematics, statics, and fault tolerance of cable-suspended robots, Journal of Robotic Systems 15 (10) (1998) 581–597.
URL https://doi.org/10.1002/(SICI)1097-4563(199810)15:10<581::AID-ROB4>3.0.CO;2-P
[31] E. Picard, S. Caro, F. Claveau, F. Plestan, Pulleys and force sensors influence on payload estimation of cable-driven parallel robots, in : 2018 IEEE/RSJ International Conference on Intelligent Robots and Systems (IROS), 2018, pp. 1429–1436.
URL https://doi.org/10.1109/IROS.2018.8594171
[32] S. Baklouti, E. Courteille, S. Caro, M. Dkhil, Dynamic and oscillatory motions of cable-driven parallel robots based on a nonlinear cable tension model, Journal of Mechanisms Robotics 9 (6).
URL https://doi.org/10.1115/1.4038068
[33] N. Binaud, S. Caro, P. Wenger, Sensitivity comparison of planar parallel manipulators, Mechanism and Machine Theory 45 (11) (2010) 1477–1490.
URL https://doi.org/10.1016/j.mechmachtheory.2010.07.004
[34] J.-P. Merlet, The kinematics of cable-driven parallel robots with sagging cables : preliminary results, in : International Conference on Robotics and Automation, 2015, pp. 1593–1598.
URL https://doi.org/10.1109/ICRA.2015.7139401
[35] M. Miyasaka, M. Haghighipanah, Y. Li, B. Hannaford, Hysteresis model of longitudinally loaded cable for cable driven robots and identification of the parameters, in : International Conference on Robotics and Automation, 2016, pp. 4051–4057.
URL https://doi.org/10.1109/ICRA.2016.7487596
[36] Z.-H. Zhu, S.-A. Meguid, Nonlinear FE-based investigation of flexural damping of slacking wire cables, International Journal of Solids and Structures 44 (16) (2007) 5122–5132.
URL https://doi.org/10.1016/j.ijsolstr.2006.12.024